Dear Prof. Dr. Hanna Lee,

We are grateful for your valuable suggestions. We also thank a lot for all comments, revisions, and suggestions from the two reviewers, which help improve our initial manuscript. Accordingly, we have made the following modifications to the manuscript.

1. We have replotted all figures. Meanwhile, we reduced the number of tables and figures by combining or moving some of them to the Appendix in the revised manuscript.

2. In the "4.3 Model uncertainties" section, we have added limitations of the current model configuration, uncertainties in the projection of permafrost degradation, and outlooks in the next work.

3. In the "2.3.1 Model description" section, we added information on the vertical resolution of our model.

4. In the "4.2 Process of permafrost degradation" section, we have added the advantage of our permafrost model in simulating permafrost thermal regime dynamics compared to other models (e.g., LSMs).

5. The full text has been carefully checked and has revised wording errors.

6. English language editing carefully by native speakers.

7. We added Dr. Yuxin Zhang (zhangyuxin201108@163.com) to the author list as he provides insightful and valuable suggestions in the process of manuscript revision.

Thank you very much for your consideration. We look forward to hearing from you.

Sincerely,

Prof. Dr. Lin Zhao

On behalf of all co-authors

Below are our one-by-one responses to these comments. The original reviewer comments are in normal black font while our answers appear in blue font. The corresponding edit in the manuscript is included in red font.

Editor's comments to the author:

The authors have done a fine job responding to the reviewers comments. Please revise the manuscript accordingly. In addition to the reviewer comments, I have two recommendations for the authors. Firstly, I encourage the authors to think about reducing the number of tables and figures by moving some of them to supplementary information or combining them. At this time, there are too many tables and figures and I suggest being more concise in tables and figures. Secondly, I suggest the authors to send the manuscript for a professional English language editing service before the final submission.

Response:

Firstly, we combined Table 4-5. Secondly, we move Table 1-2, and Figure 2-5 to the Appendix. Details of new figures are as follows:

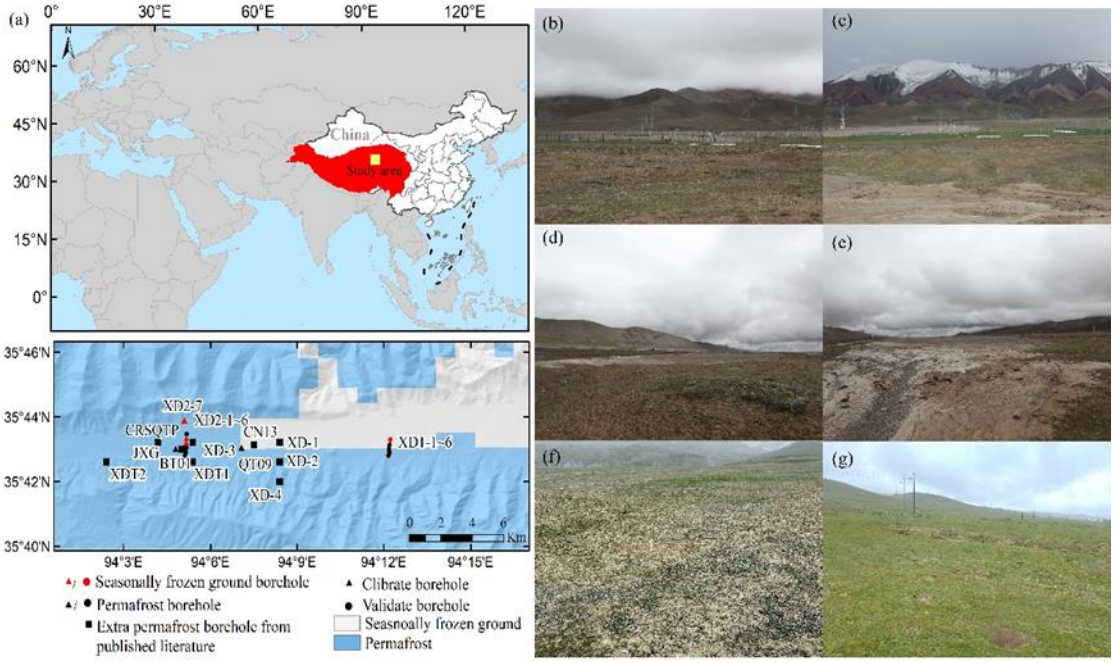

Figure 1. The geographical location of the Xidatan on the QTP, its topography and the location of 24 borehole sites (a). Surface conditions at monitoring borehole sites (b–g): view over the Xidatan comprehensive observation site (b), QT09, view towards the south (c), QT09, view towards the northeast (d), view from the vicinity of QT09 towards the east (e), XD2–1~2–7, view towards the south (f), XD1–1~1–6, view towards the east (g) (the spatial distribution of frozen ground types are derived from Zou et al. (2017); topography was generated by the Digital Elevations Model constructed (DEM) from the Shuttle Radar Topography Missions (SRTM) with a 1-arcsecond (~30 m) (Jarvis et al., 2008), Tibet Plateau boundary was from National Tibetan Plateau Data Center (Zhang et al., 2019). all photographs were taken during the field investigation from 23 July 2021 to 2 Auges 2021).

Table 1. Error metrics for the assessment of daily average ground temperature at different depths, which derived from the observed with simulated for individual calibration and validation site (good criteria values<0.2 ℃ are displayed in italics).

Criteria	Site	0.5 m	1 m	3 m	8 m	15 m	30 m
MAE	BT01	1.04	1.04	0.52	0.41	*0.19*	*0.09*
(℃)	XD2-7	2.02	1.46	0.38	*0.05*		
	QT09	1.06	0.89	0.23	*0.16*	*0.18*	*0.04*
	XD2-6	1.42	0.69	0.23	0.22	0.38	
	XD2-1	1.05	0.95	0.41	*0.13*	*0.19*	
	XD2-4	1.01	0.86	0.21	*0.14*	*0.01*	
	XD1-1	1.27	1.18	0.52	0.25	*0.19*	
	XD1-4	1.11	0.92	0.44	*0.19*	*0.08*	
RMSE	BT01	1.36	1.38	0.72	0.41	*0.19*	*0.09*
(℃)	XD2-7	2.46	1.79	0.58	*0.06*		
	QT09	1.40	1.48	0.40	*0.17*	*0.18*	*0.04*
	XD2-6	1.78	0.87	0.30	0.23	0.38	
	XD2-1	1.36	1.20	0.54	0.24	*0.19*	
	XD2-4	1.31	1.15	0.35	*0.14*	*0.02*	
	XD1-1	1.63	1.48	0.80	0.25	*0.19*	
	XD1-4	1.41	1.19	0.62	0.20	*0.08*	

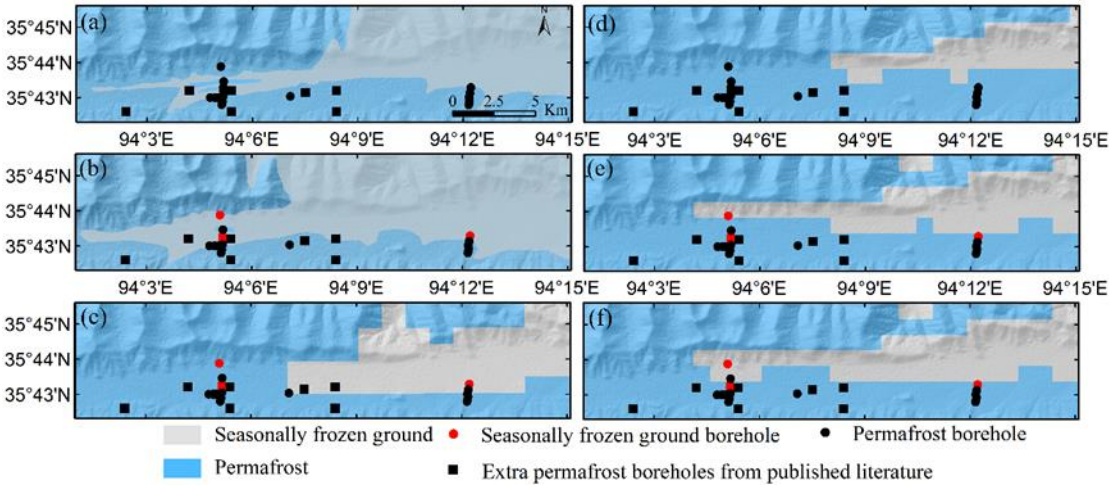

Figure 2. Geographic distribution of frozen ground type across the Xidatan for three permafrost maps accomplished in 1975, 2012 and 2016 (left panels 1975 (a), 2012 (b), 2016 (c), published in Nan et al. (2003), Luo et al. (2018) and Zou et al.(2017)) compared to corresponding modelled outputs (right panels, 1975 (d), 2012 (e), 2016 (f)).

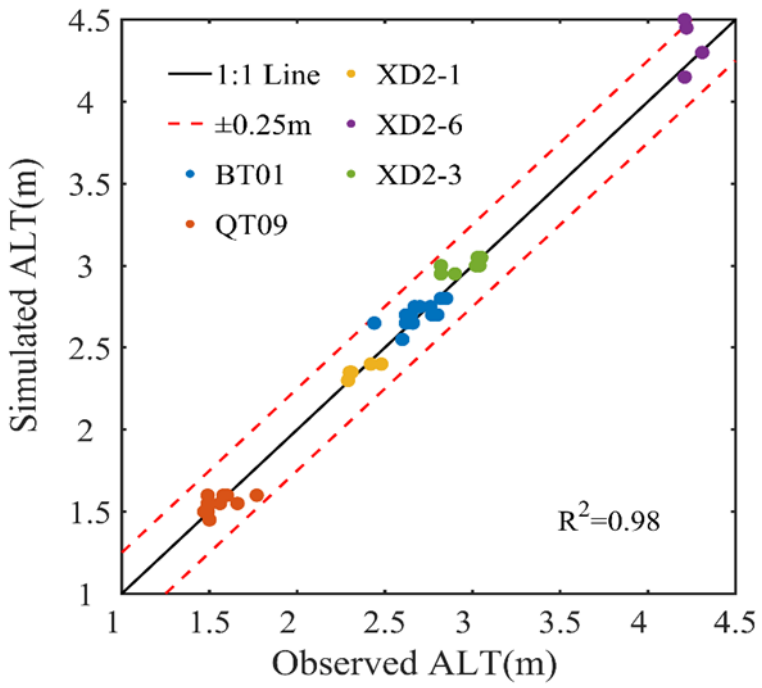

Figure 3. Comparison between annually observed ALT and simulated at different sites (the TB01 and QT09 (Liu et al. (2019), Zhao et al. (2021) observed from period 2005 to 2017, 2005 to 2018 are available, respectively, observation period at the XD2-1, XD2-3, and XD2-6 (Yin et al. (2021)) are from 2013 to 2019, 2013 to 2017, respectively. The solid line is a 1:1 line and the dashed line shows biases within ±0.25 m, dots are colored to represent the different sites).

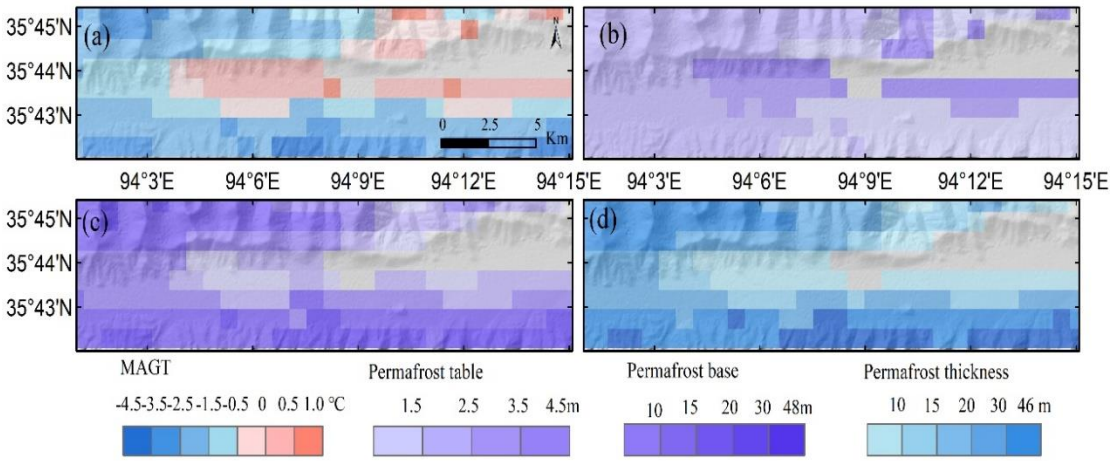

Figure 4. Spatial distributive features of MAGT (a), permafrost table (b), permafrost base (c), and permafrost thickness (d) for the initial simulation of the 1970s over the Xidatan (grey areas with the seasonally frozen ground were excluded).

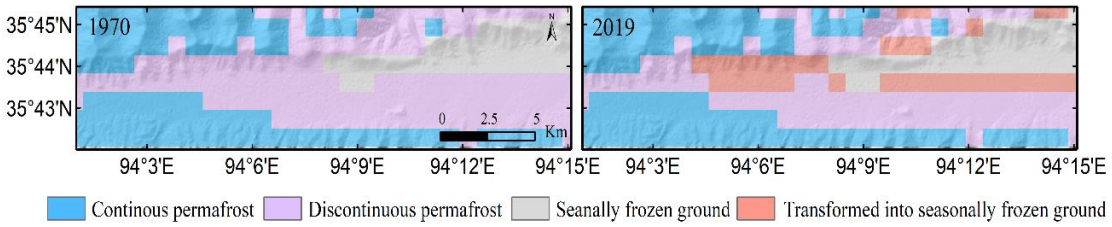

Figure 5. Spatial distributive changes of frozen ground type over the Xidatan from 1970 to 2019.

Table 2. Variations of the permafrost boundary and areal extent of frozen ground type over the Xidatan for 1970-2019, and that of projected variations by 2100 under different climate change scenarios.

	The lower limit or the lowest elevation of permafrost boundary (m a.s.l.)		Areal extent (%)		
	North–facing	South–facing	Con.	Disc.	Seas.
1970	4525(4138)	4732 (4357)	33.93	46.07	20.00
2019	4525 (4185)	4732 (4357)	33.93	33.21	32.86
SSP1–2.6 (2100)	4567 (4308)	4732 (4516)	28.57	30.36	41.07
SSP2–4.5 (2100)	4567 (4308)	4732 (4516)	28.57	28.57	42.86
SSP5–8.5 (2100)	4567 (4309)	4754 (4570)	27.14	21.79	51.07
RCP2.6 (2100)	4567 (4308)	4732 (4416)	28.57	30.36	41.07
RCP4.5 (2100)	4567 (4308)	4732 (4516)	29.29	27.50	43.21
RCP8.5 (2100)	4567 (4309)	4737 (4558)	28.93	22.50	48.57

Note: Outside brackets were the lower limit of the continuous permafrost zone, while in brackets were the lowest elevation of the permafrost boundary. Con., Disc., and Seas. are indicated as continuous permafrost, discontinuous permafrost, and seasonally frozen ground, respectively.

Table 3. Changes in characteristics of frozen ground type over the Xidatan for the period 1970 to 2019, and projected changes by the 2090s, relative to the 2010s, under different climate change scenarios.

	Types	1970–2019	SSP1–2.6	SSP2–4.5	SSP5–8.5	RCP2.6	RCP4.5	RCP8.5
MAGT (°C)	Con.	0.49	0.73	0.94	1.03	0.65	0.91	1.06
	Disc.	0.40	0.53	0.66	0.96	0.48	0.65	0.86
Permafrost table (m)	Con.	0.37	0.56	1.76	6.24	0.44	1.23	4.95
	Disc.	0.35	0.87	3.13	7.02	0.64	2.26	6.13
Permafrost base (m)	Con.	-0.80	-3.52	-3.87	-3.99	-3.41	-3.81	-4.13
	Disc.	-1.60	-4.87	-5.09	-5.17	-4.80	-5.08	-5.17
Permafrost thickness (m)	Con.	-1.18	-4.11	-5.23	-10.38	-3.87	-5.11	-9.42
	Disc.	-1.96	-5.78	-7.94	-12.76	-5.46	-7.44	-11.65

Note: Con., Disc., and Seas. are indicated as continuous permafrost, discontinuous permafrost, and seasonally frozen ground, respectively.

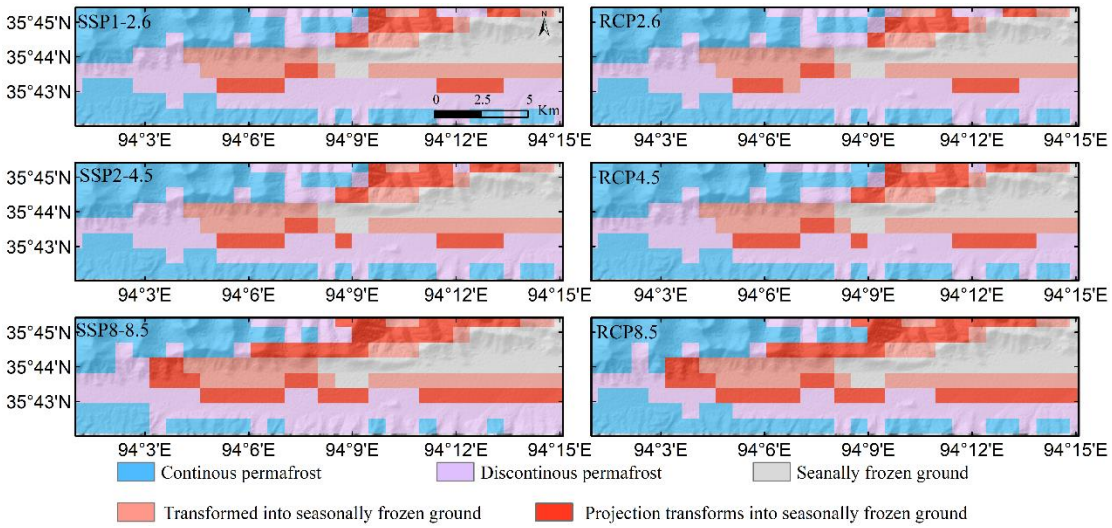

Figure 6. Projected spatial distributive changes of frozen ground type over the Xidatan in the future period by 2100 under RCPs and SSPs scenarios (left column, from top to bottom, each row shows under SSP1–2.6, SSP2–4.5, and SSP5–8.5 scenarios, right column, from top to bottom, each row shows under RCP2.6, RCP4.5, and RCP8.5 scenarios).

Appendix A

Table A1. A list of monitoring boreholes in the study area and a summary of the ground properties are shown.

Borehole (altitude/ m a.s.l.)	Coordinates	Sensor depths (m)	Frozen ground type	Soil stratigraphy
QT09 (4538)	35°43′02″ 94°07′05″	0.5–5 m (0.5 m intervals) 5–20 m (1 m intervals) 20–30 m (2 m intervals)	Permafrost	Loam (0–0.2 m) Sandy loam (0.2–1.4 m) Sandy loam with gravel (1.4–2.4 m) Sandy with gravel (2.4–10 m) Rock (10–21 m)
TB01 (4530)	35°43′00″ 94°04′09″	Same as QT09	Permafrost	Sandy loam (0–1.2 m) Sand (1.3–3 m) Sand with gravel (3–10 m) Weathered mudstone (>10 m)
XD1–1 (4379)	35°41′55″ 94°12′05″	0.5–10 m (0.5 m intervals) 10–15 m (1 m intervals)	Permafrost	Sandy cobble (0–4.5 m) Fluvial sand (4.5–15 m)
XD1–2 (4377)	35°41′59″ 94°12′07″	Same as XD1–1	Permafrost	Sandy cobble (0–4.5 m) Fluvial sand (4.5–15 m)
XD1–3 (4576)	35°42′04″ 94°12′07″	Same as XD1–1	Permafrost	Sandy cobble (0–5 m) Fluvial sand (5–15 m)

XD1–4 (4374)	35°42′10″ 94°12′07″	Same as XD1–1	Permafrost	Sandy cobble (0–5.5 m) Fluvial sand (5.5–15 m)
XD1–5 (4370)	35°42′16″ 94°12′08″	0.5–8 m (0.5 m intervals)	Permafrost	Sandy cobble (0–5.5 m) Fluvial sand (5.5–10 m)
XD1–6 (4368)	35°42′24″ 94°12′09″	Same as XD1–5	Seasonally frozen ground	Sandy cobble (0–4.5 m) Fluvial sand (4.5–8 m)
XD2–1 (4508)	35°41′56″ 94°05′08″	Same as XD1–1	Permafrost	Sand (0–2.5 m) Sand with massive ground ice (2.5–7 m) Clay (7–9 m) Weathered mudstone (9–15 m)
XD2–2 (4503)	35°42′01″ 94°05′09″	Same as XD1–1	Permafrost	Sand (0–2.8m) Sand with massive ground ice (2.5–6 m) Weathered mudstone (6–15 m)
XD2–3 (4500)	35°42′10″ 94°05′09″	Same as XD1–1	Permafrost	Sand cobble (0–4 m) Fluvial sand (4–15 m)
XD2–4 (4498)	35°42′18″ 94°05′09″	Same as XD1–1	Seasonally frozen ground	Sandy cobble (0–4 m) Fluvial sand (4–15 m)
XD2–5 (4493)	35°42′26″ 94°05′10″	Same as XD1–1	Seasonally frozen ground	Sandy cobble (0–4 m) Fluvial sand (4–15 m)
XD2–6 (4490)	35°42′36″ 94°05′11″	Same as XD1–1	Permafrost	Sandy cobble (0–4 m) Fluvial sand (4–15 m)
XD2–7 (4492)	35°43′00″ 94°05′05″	Same as XD1–5	Seasonally frozen ground	Sand (0–4.5 m) Sandstone (4–8 m)
JXG (4530)	35°43′12″ 94°04′01	1–10 m (1 m intervals) 10–30 m (2 m intervals) 0.4 m 1.6 m	Permafrost	--
CRSQTP (4530)	35°43′ 94°05′	4–10 m (2 m intervals) 10–18 m (4 m intervals) 18–20 m (2 m intervals) 20–29 m (3 m intervals)	Permafrost	--
XD1 (4427)	35°43′12″ 94°08′24″	--	Permafrost	--
XD2 (4530)	35°43′12″ 94°04′14″	--	Permafrost	--
XD3 (4480)	35°43′12″ 94°05′24″	--	Permafrost	--
XD4	35°42′00″	--	Permafrost	--

(4427)	94°08′24″			
XDT1	35°42′36″	--	Permafrost	--
(4602)	94°02′24″			
XDT2	35°42′36″	--	Permafrost	--
(4530)	94°05′24″			
CN13	35°42′12″	--	Permafrost	--
(4448)	94°07′48″			

Note: The symbol--is field-observed frozen ground types collected from previously published literature (Wang et al., 2000; Jin et al., 2000,2006; Cheng et al., 2007).

Table A2. Calibration thermophysical parameters of different soil layers used for soil temperature modelling.

Texture	*K* (W m^{-1} °C^{-1})		*C* (kJ m^{-3} °C^{-1})		VWC (%)
	Frozen	Thawed	Frozen	Thawed	
Loam	1.25–1.57	0.85–1.28	1639–1879	2208–2475	15–20
Clay	0.83–1.30	0.61–1.03	1756–1907	1881–2191	15–20
Sandy loam	1.31–1.93	1.17–1.71	1844–2107	2258–2634	10–20
Loamy sand	1.02–1.38	1.11–1.24	2040–2208	2541–2676	15–20
Sand cobble	1.0–1.29	0.89–1.10	1639–1739	2007–2208	13–15
Fluvial sand	1.32–1.60	1.09–1.30	1288–1413	1568–1819	6–10
Sand	1.86–2.15	1.48–1.64	1505–1639	1940–2208.1	10–14
Sandstone	0.94–1.91	0.77–1.47	1317–1459	1493–1777	2–6
Sand with Gravel	1.91–2.20	1.47–1.68	1459–1601	1777–2061	6–10
Weathered mudstone	2.27	1.71	1543	1881	6
Rock	0.33	0.33	1940	1940	2

Note: *K* is the thermal conductivity; *C* is the volumetric heat capacity; as well as *VWC* represents total volumetric water/ice content. Soil texture information from Luo et al. (2018) and Liu et al. (2021), the values of thermal conductivity and heat capacity were from Construction of Ministry of PRC. (2011) and Yershov. (2016), and fine–adjusted during the calibration, water content was determined by the soil samples of the borehole cores combined with the observation dataset vicinity of QT09 and the ground ice distribution maps from Zhao et al. (2010).

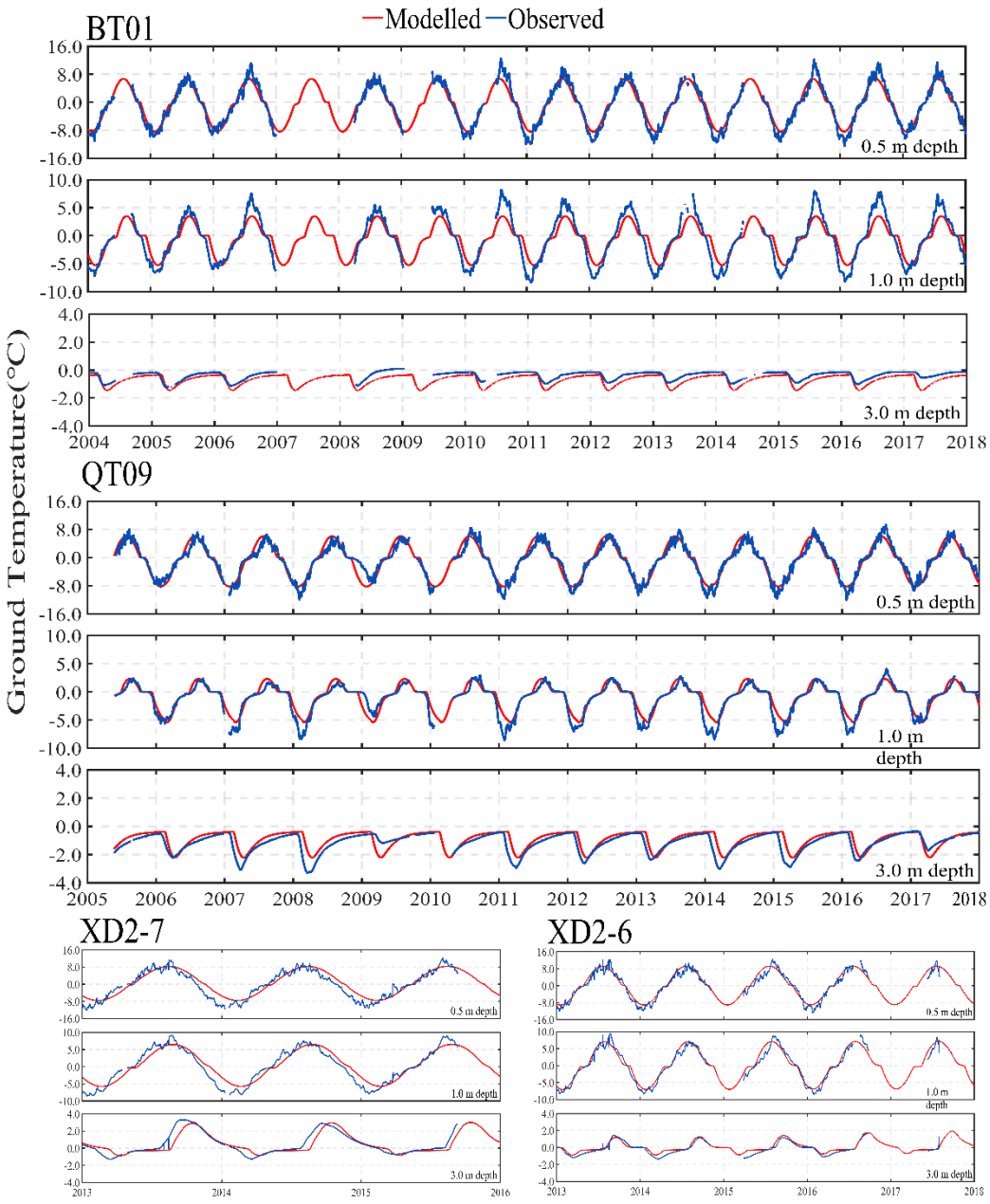

Figure A1. Comparison of the simulated (red lines) to observed (blue lines) daily mean ground temperature at 0.5 m, 1.0 m, 3.0 m depth in four calibration boreholes (BT01, XD2-7, QT09, and XD2-6) during the observation period (There were some data gaps due to temperature probe failure in some years, at the BT01, the data gaps in the record mainly occurred at 0.5-15 m in 2007-2008, and at 15-30 m during the 2005-2007 and 2011-2018, at the QT09, observations at 15-30 m of 2006-2008, 2011-2013, and 2015-2018 are not available, at the XD2-6, the data gap in the record in 2016-2017).

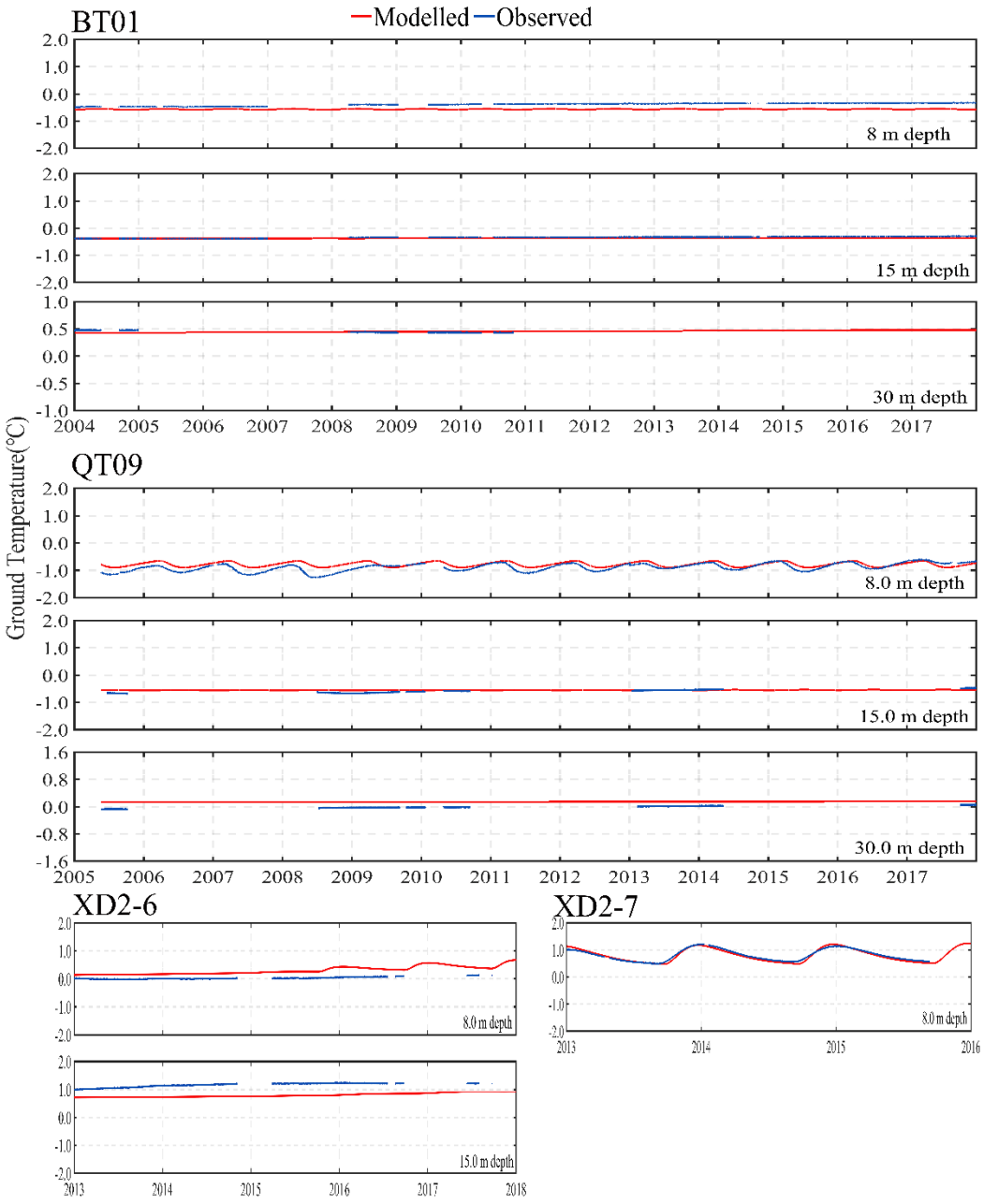

Figure A2. Same as Figure 2. but for daily mean ground temperature at 8 m, 15 m, and 30 m.

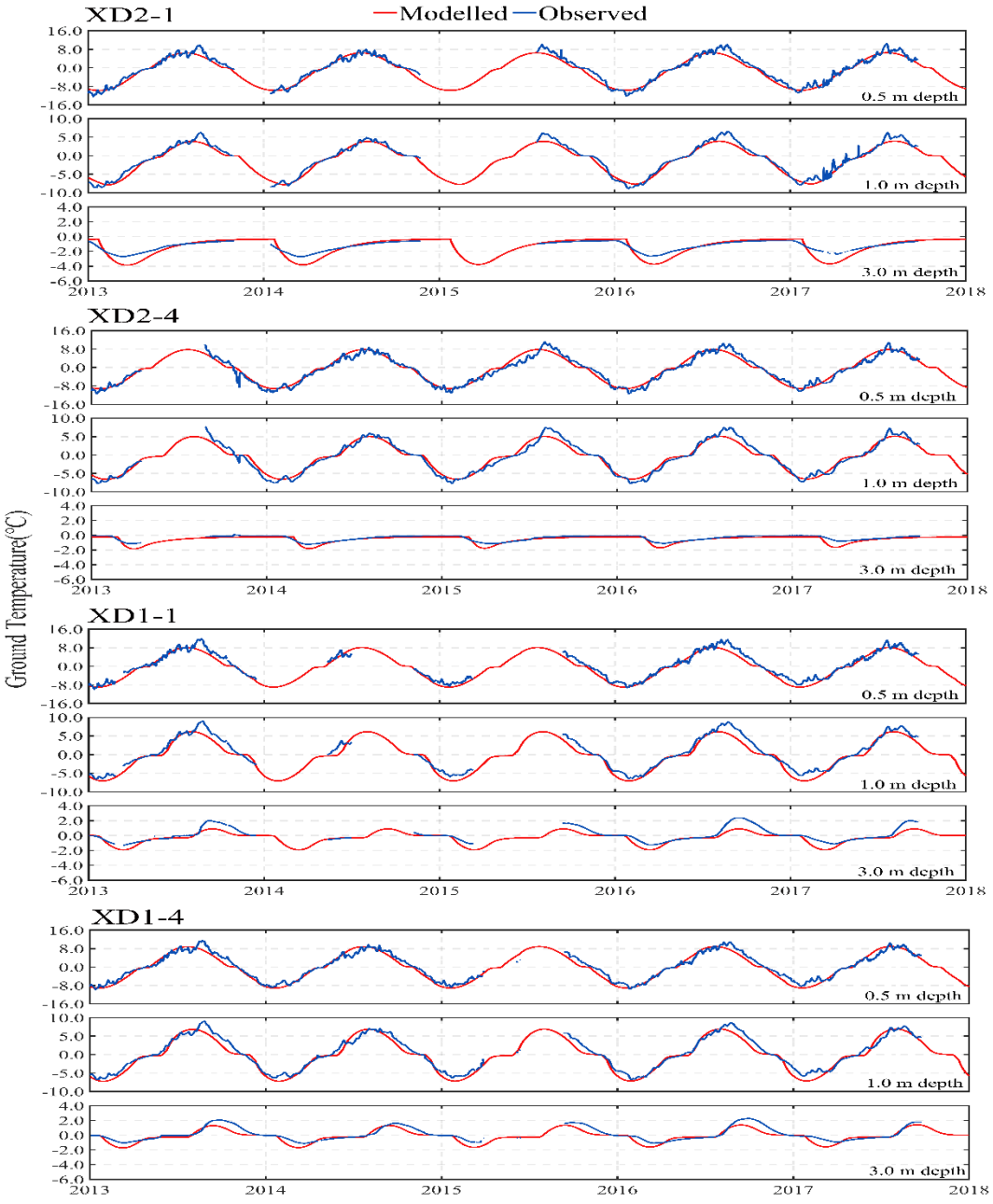

Figure A3. Comparison of the simulated (red lines) to observed (blue lines) daily mean ground temperature at 0.5 m, 1.0 m, and 3.0 m depth in four validation boreholes (XD2-1, XD2-4, XD1-1, and XD1-4) during the observation period from 2013 to 2018 (There were some data gaps due to temperature probe failure in some years, at the XD2-1, the data gaps in the record mainly occurred at 0.5-3.0 m in the first half of 2015, at the XD1-1, the data gap in the record at 0.5-3.0 in 2014-2015, at 8-15 m during the 2013-2015, at the XD1-4, the data gap in the record in the first half of 2015).

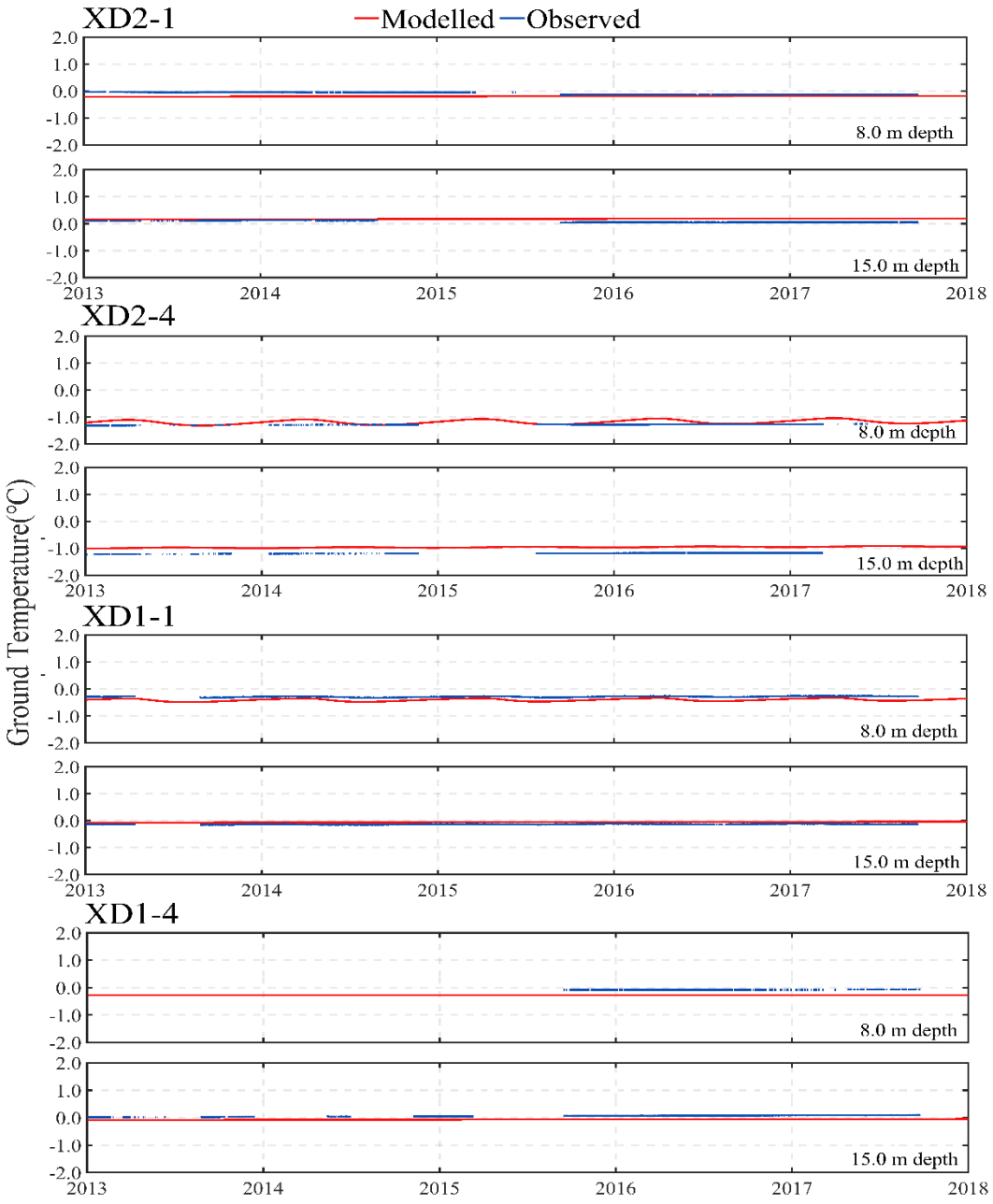

Figure A4. Same as Figure 4. but for daily mean ground temperature at 8 m, and 15 m.

Response to Reviewer#1

Review of "Simulation of the current and future dynamics of permafrost near the northern limit of permafrost on the Qinghai–Tibet Plateau" By Zhao et al.

This study simulates the thermal state and its dynamics of permafrost over a small region near the northern limit on the Qinghai-Tibet Plateau (QTP) where the permafrost is a fragile state. The simulation relies on a model developed from numerically solving the one-dimensional transient Fourier's law heat conduction equation. The model has taken several important biogeophysical processes, such as the phase change of soil water, into consideration for a better reproduction of the soil temperature field. The model is carefully validated and calibrated over the study area using meteorology and borehole data. As the result, the validated and calibrated model successfully improve the simulation of the spatial-temporal distribution/variation of permafrost thermal state over the study area, The model is then forced by CMIP5/CMIP6 projection data under the scenario of RCPs and SSPs. The warming rate of permafrost is slightly higher in the SSP scenario than in the RCP scenario. This study highlights the slow delaying process of the mountain permafrost in response to the warming climate. In general, this model-based study is well-shaped with model development, model evaluation/calibration, and model application/projection. The newly-developed model provides a new tool in estimating the response of mountain permafrost in the QTP to the warming climate, supporting new studies to the observational results. Overall, I recommend an acceptance after addressing some minor revisions.

Response:

Thanks a lot for all the comments, revisions and suggestions, especially for your positive comment on our work. We provide our responses one by one to the comments. The original reviewer comments are in normal black font while our answers appear in bule font. The corresponding edit in the manuscript are included in red font.

Major issues:

The resolution of this modeling study is relatively high (1km), and the model configuration is totally one-dimensional. So, in my opinion, the model biases resulted from ignoring the horizontal fluxes of heat and water should not be ignored any more under such a fine grid spacing. Considering the complex topography in the study area, authors should do more in estimating the model uncertainty because of the ignorance of horizontal heat and water fluxes.

Response:

It is a real issue to pay more attention for ignoring the horizontal heat and water fluxes during simulation, and it would be more important for simulate the water cycles in such regions than the heat dynamics. Our answer is:

Firstly, our model reasonably reproduces the vertical ground temperature profile, and active layer thickness is in good agreement with the observation for the last 10 years. The good model performance might be compensated by the calibration parameters. We also believe that the one-

dimensional heat flow model can realistically capture the dominating processes of vertical heat transfer processes because the lateral conductive heat into and out of every simulated pixel (1 km) must be much low, and even to nearly balanced, which is due to the much smaller lateral temperature gradient. These facts are strongly corroborating the effect of lateral heat fluxes by Etzelmüller et al. (2011), Jsfarov et al. (2012), Hipp et al. (2012), and Westermann et al. (2013).

Secondly, Xidatan region is in a faulted valley with relatively gentle topography (slopes of ~90% of areas are lower than 5°). The heat transfer caused by lateral groundwater fluxes in and out the simulated pixel would be nearly balanced in most parts of this area, and the effect of this kind of lateral heat fluxes caused by water fluxes thus is considered minor and does not have a significant role in these regions. But small areas of flood land in the valley, where high spatial heterogeneity of surface condition, includes fine particle soil with relatively high soil hydraulic conductivity. In these regions, the transfer process of lateral water fluxes may exist in the active layer and play a crucial role in the ground thermal regime (Bense et al., 2012; Sjöberg et al., 2016; Kurylyk et al., 2016). The impact of this local hydrological process on permafrost thermal regimes is unknown at the current model configuration, but investigations into hydrogeological processes will form the basis of future work.

In the revised manuscript, we added a supplement to the description of the current uncertainties of model and future improvements in the discussion section. The text there reads as:
"*Note that the limitation of the current model is one-dimensional, which assumes each grid cell to be uniform without lateral exchange. Our simulations, therefore, are considered as conservatively changes in the ground temperature in areas with lateral water fluxes, such as flood land in the valley. The representation of the horizontal fluxes exchange of heat and water deserves increased attention in future modeling approaches, and coupling the current model with this physical process of heat transfer could be an important step toward better simulation results of high-resolution in the next generation of permafrost models.*"

In any way, we will try to do more work on the issues raised by the reviewers.

Reference:

Etzelmüller, B., Schuler, T., Isaksen, K., Christiansen, H., Farbrot, H., and Benestad, R.: Modeling the temperature evolution of Svalbard permafrost during the 20th and 21st century, The Cryosphere, 5, 67-21, https://doi.org/10.5194/tc-5-67-2011, 2011.

Jafarov, E., Marchenko, S., and Romanovsky, V.: Numerical modeling of permafrost dynamics in Alaska using a high spatial resolution dataset, The Cryosphere, 6, 613-624, https://doi.org/10.5194/tc-6-613-2012, 2012

Hipp. T., Etzelmüller, B, Farbrot, H., Schuler, T., and Westermann, S.: Modelling borehole temperatures in Southern Norway–insights into permafrost dynamics during the 20th and 21st century, The Cryosphere, 6, 533-571, https://doi.org/10.5194/tc-6-553-2012, 2012.

Westermann, S., Schuler, T., Gisnås, K., and Etzelmüller, B.: Transient thermal modeling of permafrost conditions in Southern Norway, The Cryosphere 7, 719-739, https://doi.org/10.5194/tc-7-719-2013, 2013

Wu, T., Li, S., Cheng, G., and Nan, Z.: Using ground-penetrating radar to detect permafrost degradation in the northern limit of permafrost on the Tibetan plateau, Cold Reg. Sci. Technol., 41,211-219, https://doi.org/10.1016/j.coldregions.2004.10.006, 2005.

Luo, J., Niu, F., Lin, Z., Liu, M., and Yin, G.: Variations in the northern permafrost boundary over the last four decades in the Xidatan region, Qinghai–Tibet Plateau. J. Mt. Sci., 15, 765–778, https://doi.org/10.1007/s11629-017-4731-2, 2018.

Bense, V., Kooi, H., Ferguson, G., Read, T.: Permafrost degradation as a control on hydrogeological regime shifts in a warming climate, J Geophys Res Earth Surf 117. https://doi.org/10.1029/2011JF002143, 2012.

Sjöberg, Y., Coon, E., Sannel, A., Pannetier, R., Harp, D., Frampton, A., Painter, S., Lyon SW.: Thermal effects of groundwater flow through subarctic fens: a case study based on field observations and numerical modeling, Water Resour Res 52:1591–1606.https://doi.org/10.1002/2015WR017571, 2016.

Kurylyk, BL., MacQuarrie, K., Voss, C.: Climate change impacts on the temperature and magnitude of groundwater discharge from shallow, unconfined aquifers, Water Resour Res, 50:3253–3274 ,2014b.

Minor comment:

Section 2.3.1 What is the vertical resolution of your soil model?

Response:

In our simulations, each grid cell on the map uses a one-dimensional multilayer soil profile down to the depth of 100 m. The vertical grid has fine resolution between nearby point at the near ground layer (0.05m) and become coarse towards the bottom boundary (0.5m). More detailed description, readers are kindly referred to previously published literature in PPP and GRL by Sun et al. (2019 and 2022).

We have added relevant description in section 2.3.1 in the revised manuscript. The text there read as: "*With comprehensive consideration of the modeling precision and computation cost, we choose the calculate time step to be one day, and set a total of 282 vertical levels for each soil column, with the vertical resolution configurations of 0.05m (the upper 4 m) and 0.5m (remaining soil layer to 100 m).*"

Reference

Sun, Z., Zhao, L., Hu, G., Qiao, Y., Du, E., Zou, D., and Xie, C.: Modeling permafrost changes on the Qinghai-Tibetan plateau from 1966 to 2100: a case study from two boreholes along the Qinghai-Tibet engineering corridor. Permafrost and Periglac. Process., 32:156-171, https://doi.org/10.1002/ppp.2022, 2019.

Sun, Z., Zhao, L., Hu, G., Zhou, H., Liu, S., Qiao, Y., Du, E., Zou, D., and Xie, C.: Numerical

simulation of thaw settlement and permafrost changes at three sites along the Qinghai-Tibet Engineering Corridor in a warming climate, Geophysical Research Letters, 49, e2021GL097334, https://doi.org/10.1029/2021GL097334, 2022.

Line 320: I suppose the warming rate of SSP245 should be 0.032 instead for 0.32.

Response:

We have changed in the revised manuscript. The text there reads as: "*0.032℃ a^{-1}(SSP2-4.5, moderate mitigation)*".

Line 348: The single quotation mark in "model's performance evaluation" is not correct.

Response:

We have changed in the revised manuscript. The text there reads as: "*model's performance evaluation*".

Fig. 2-5. I have several questions concerns about the results shown by these figures on model evaluation.

- How do you explain the better permafrost of model in reproducing the soil temperature in the shallow layers than that in the deep layers (8m and 15m) for some sties?

Response:

This is just a special case in some areas, where complex surface conditions. The deviation between measured and simulated soil temperature in this special case might be caused by micro-scale heterogeneity in terms of surface cover, topography, and soil stratigraphy at the sub-grid scale. For example, XD2-6 has relatively poor performance compared with other sites. It may be attributed to being located at the edge of the island permafrost of river erosion area with high spatial heterogeneity of surface conditions (Luo et al., 2018; Yin et al., 2021). However, the deviation between the modelled results and measured values for this site within 0.38℃ at the deep layer (15 m), superior to other models, such as LSMs. Furthermore, island permafrost was simulated to disappear in the mid-late 2010s, which was reasonable and in compliance with direct observation facts (Yin et al., 2021). We can conclude that various depths of ground temperature simulated by our model are still satisfactory for this site. On the other hand, the coordinate range of the graph is not adjusted well so that some sites seem to have a larger error in the deep layer. We have modified Fig. 2-5 in the revised manuscript.

We added a supplement in the "3.1 model's performance evaluation" section in our revised manuscript, the text there reads as "*Site XD2–6 has relatively poor performance compared with other sites, it might be caused by micro-scale heterogeneity in terms of surface cover, topography, and soil stratigraphy at the sub-grid scale, leading to more difficulty in accurate modeling.*"

Reference

Yin, G., Luo, J., Niu, F., Lin, Z., and Liu, M.: Thermal regime and variations in the island permafrost

near the northern permafrost boundary in Xidatan, Qinghai–Tibet Plateau, Front. Earth Sci., 560, https://doi.org/10.3389/feart.2021.708630, 2021.

Luo, J., Niu, F., Lin, Z., Liu, M., and Yin, G.: Variations in the northern permafrost boundary over the last four decades in the Xidatan region, Qinghai–Tibet Plateau. J. Mt. Sci., 15, 765–778, https://doi.org/10.1007/s11629-017-4731-2, 2018.

- Why in Fig.3 and 5, there are discontinuity of time series for modelled temperature while no discontinuity in observed results, which is against common sense.

Response:

We reversed the legend of simulation and observation, sorry for the mistake, and we have corrected the mistake in new figures.

- I recommend to use dotted line rather than dashed line for modeled time series since the dashed lines cannot clearly show the annual peak temperature.

Response:

Fig. 2-5 have been modified to make the contrast clearer.

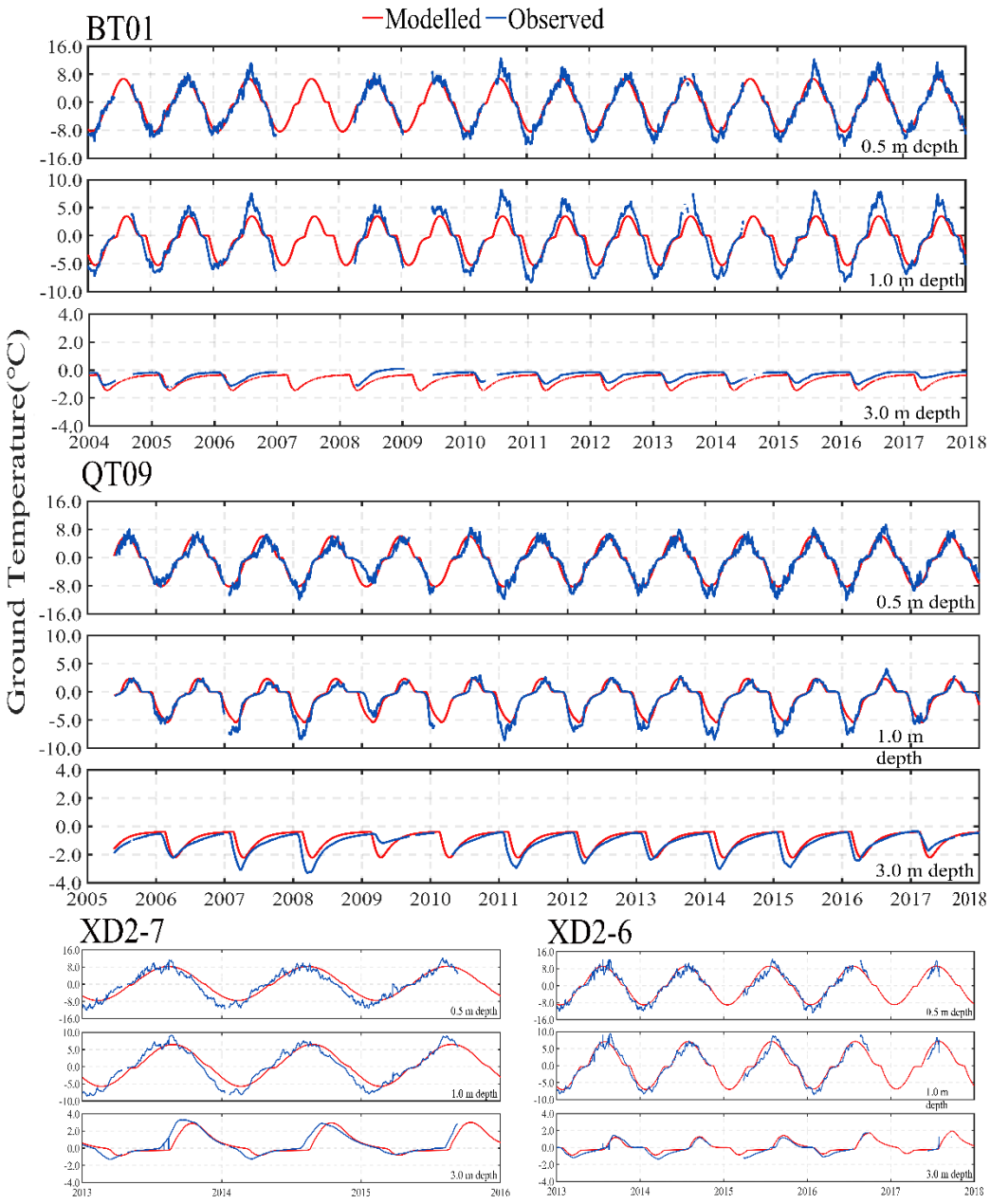

Figure 2. Comparison of the modelled (red lines) to observed (blue lines) daily mean ground temperature at 0.5 m, 1.0 m, 3.0 m depth in four calibration boreholes (BT01, XD2-7, QT09, and XD2-6) during the observation period (There were some data gaps due to temperature probe failure in some years, at the BT01, the data gaps in the record mainly occurred at 0.5-15 m in 2007-2008, and at 15-30 m during the 2005-2007 and 2011-2018, at the QT09, observations at 15-30 m of 2006-2008, 2011-2013, and 2015-2018 are not available, at the XD2-6, the data gap in the record in 2016-2017).

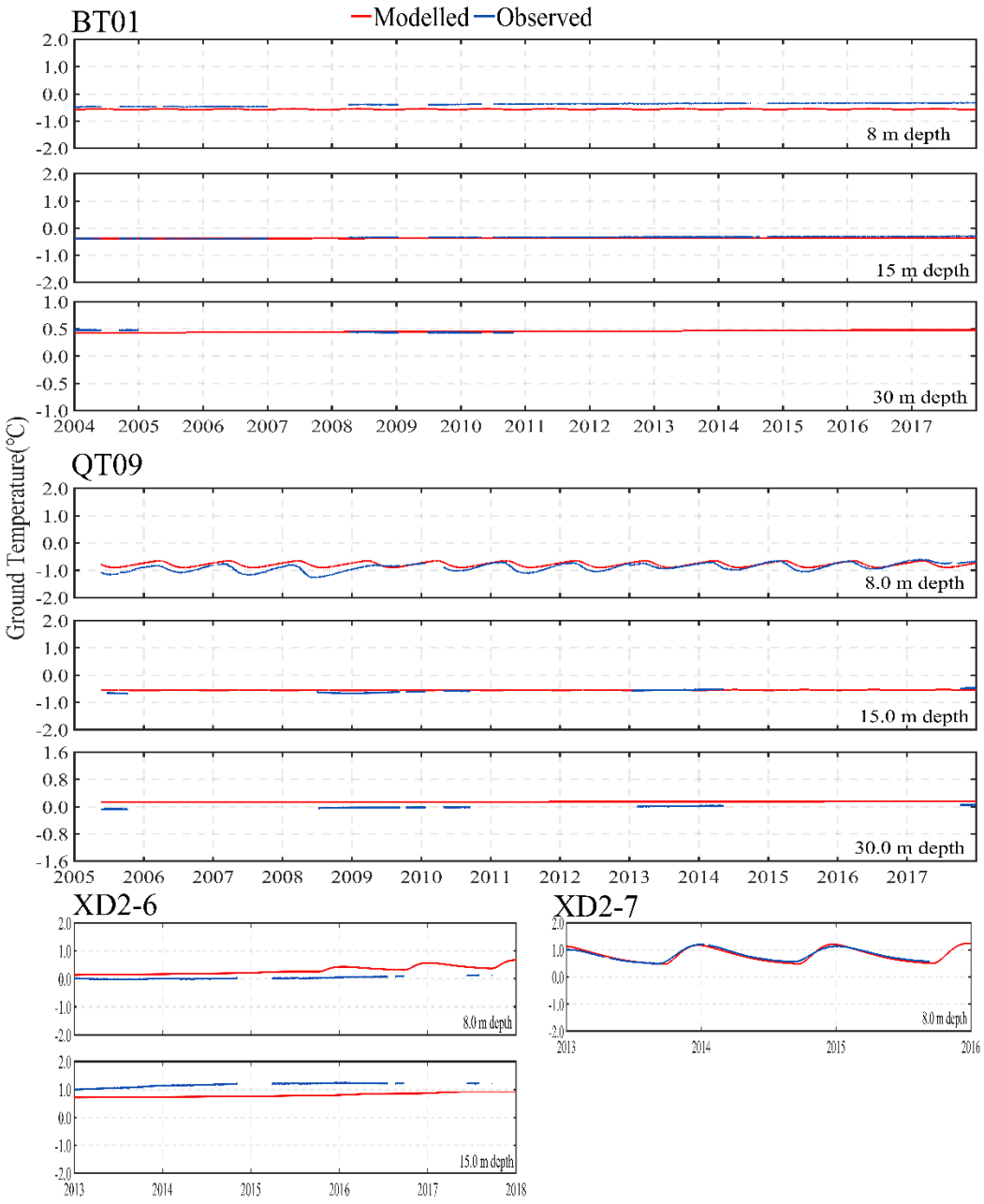

Figure 3. Same as Figure 2. but for daily mean ground temperature at 8 m, 15 m, and 30 m.

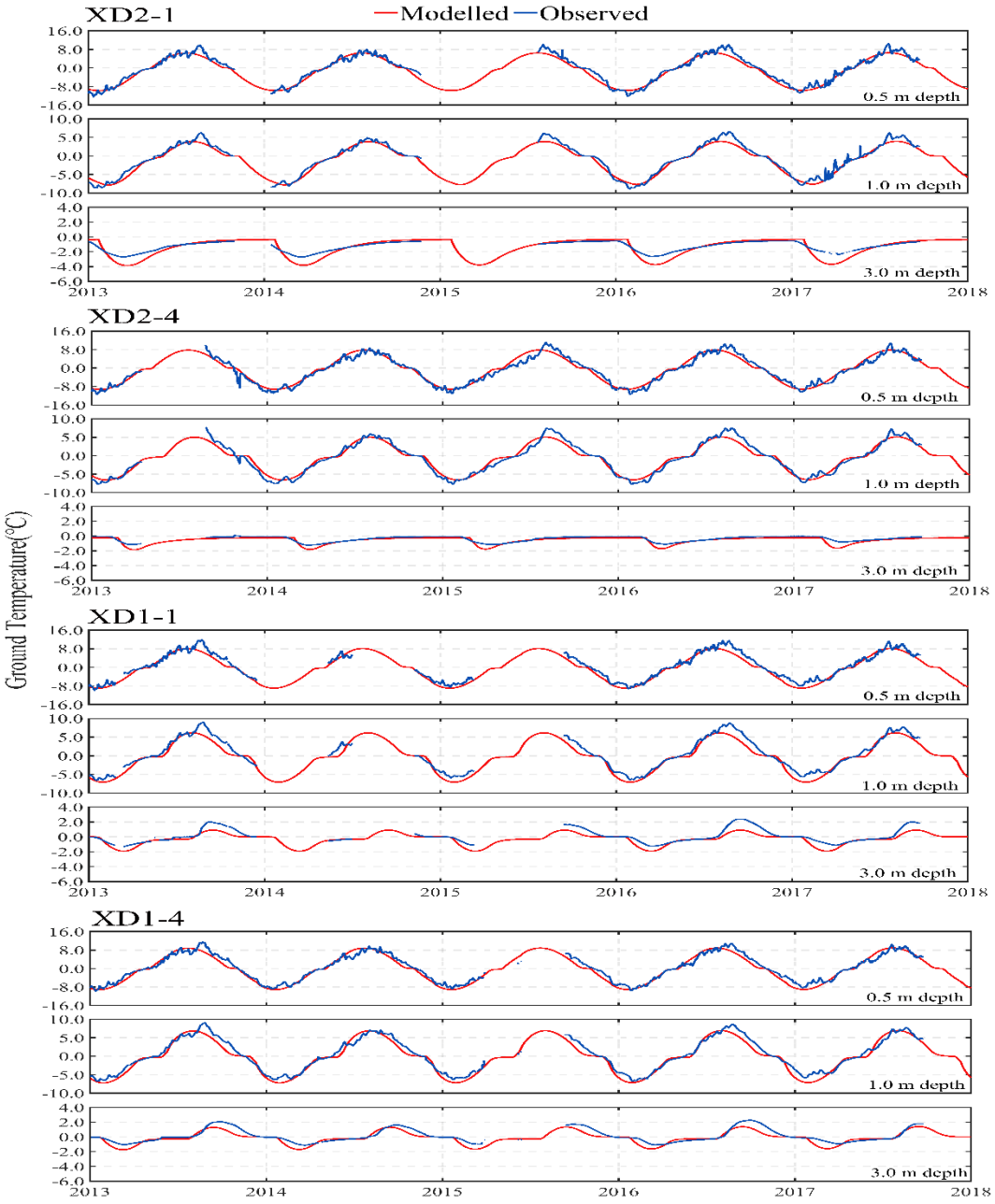

Figure 4. Comparison of the simulated (red lines) to observed (blue lines) daily mean ground temperature at 0.5 m, 1.0 m, and 3.0 m depth in four validation boreholes (XD2-1, XD2-4, XD1-1, and XD1-4) during the observation period from 2013 to 2018 (There were some data gaps due to temperature probe failure in some years, at the XD2-1, the data gaps in the record mainly occurred at 0.5-3.0 m in the first half of 2015. At the XD1-1, the data gap in the record at 0.5-3.0 in 2014-2015, at 8-15 m during the 2013-2015. At the XD1-4, the data gap in the record in the first half of 2015).

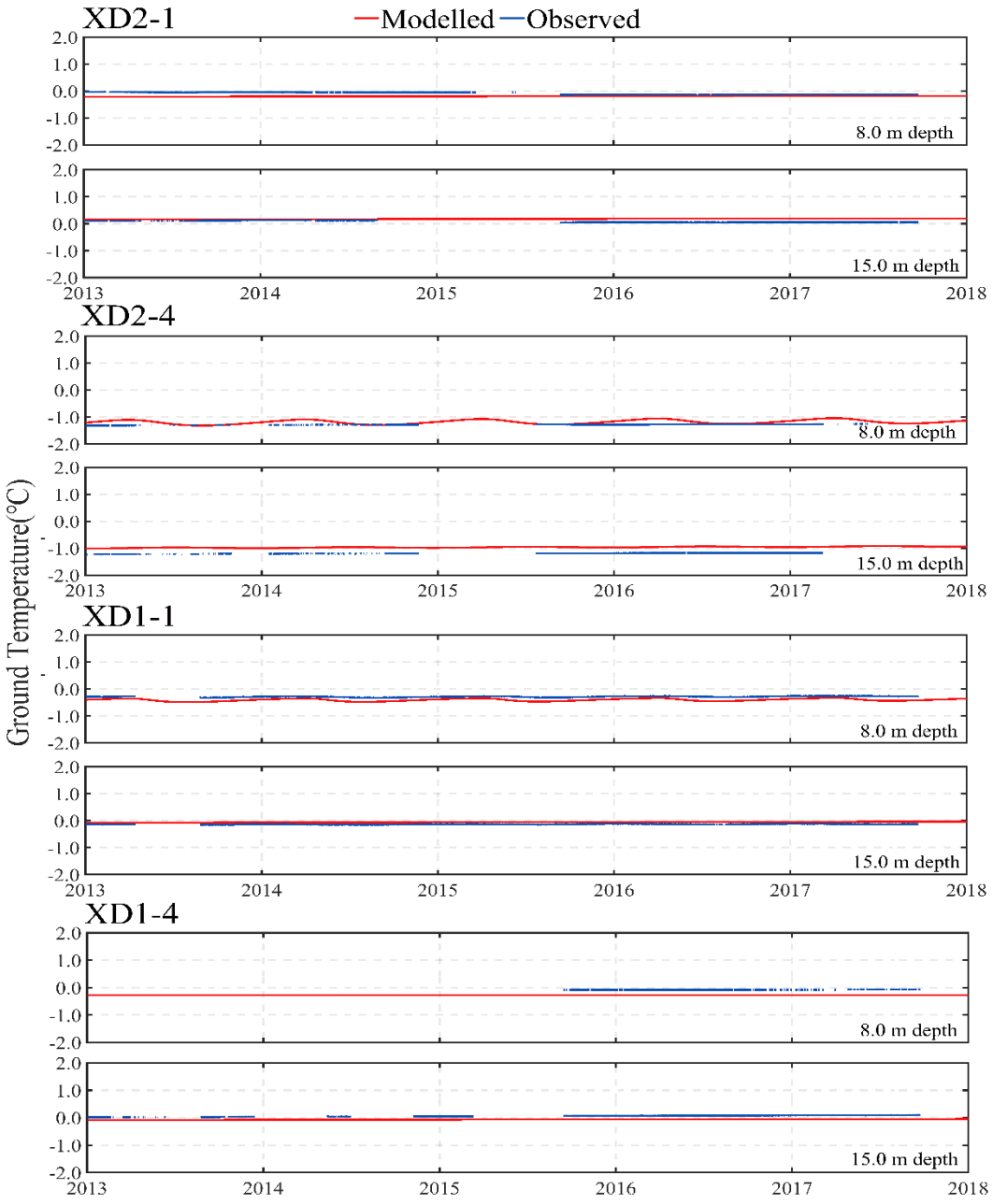

Figure 5. Same as Figure 4. But for daily mean ground temperature at 8 m, and 15 m.

Fig.6, 8, 9, and 10. For these spatial patterns, some of them has while line for topography, while some do not. I recommend to add topography in all figures.

Response:

We have added topography in all figures in the revised manuscript. The details are as follows:

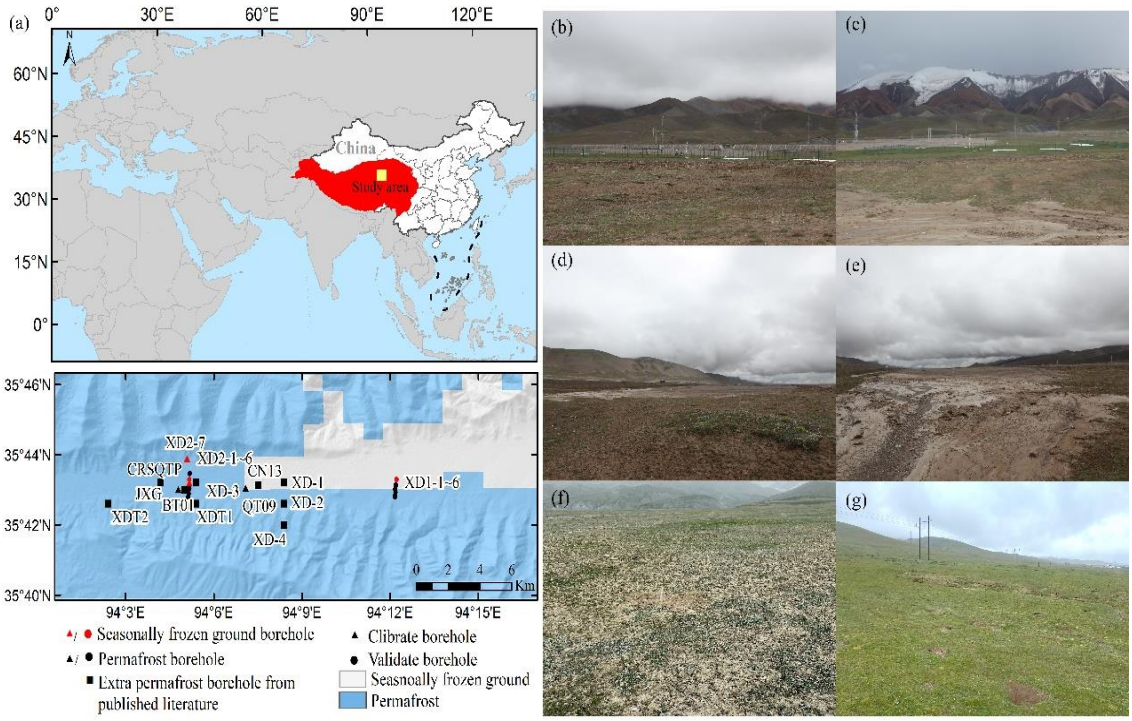

Figure 1. Geographical location of the Xidatan on the QTP, and its topography as well as the location of 24 borehole sites (a). Surface condition at monitoring borehole sites in the study area (b–g): view over the Xidatan comprehensive observation site (b), QT09, view towards the southern (c), QT09, view towards the northeast (d), view from the vicinity of QT09 towards the east (e), XD2–1~2–7, view towards the south (f), XD1–1~1–6, view towards the east (g) (the spatial distribution of permafrost is derived from Zou et al. (2017); topography was generated by the Digital Elevation Model constructed (DEM) from the Shuttle Radar Topography Missions (SRTM) with a 1-arcsecond (~30 m) (Jarvis et al., 2008), all photographs were taken during the field investigation from 23 Jul. 2021 to 2 Aug. 2021).

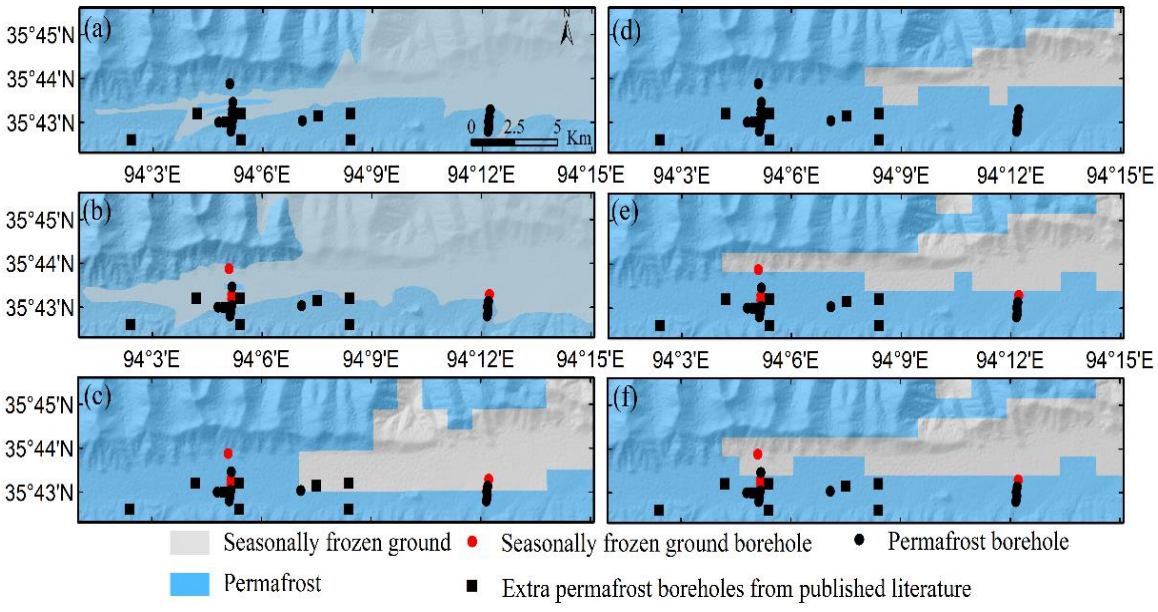

Figure 6. Geographic distribution of permafrost and seasonally frozen ground across the Xidatan for three

permafrost maps accomplished in 1975, 2012, and 2016 (left panels 1975 (a), 2012 (b), 2016 (c), published in Nan et al. (2003), Luo et al. (2018) and Zou et al. (2017)) compared to corresponding modeled outputs (right panels, 1975 (d), 2012 (e), 2016 (f)).

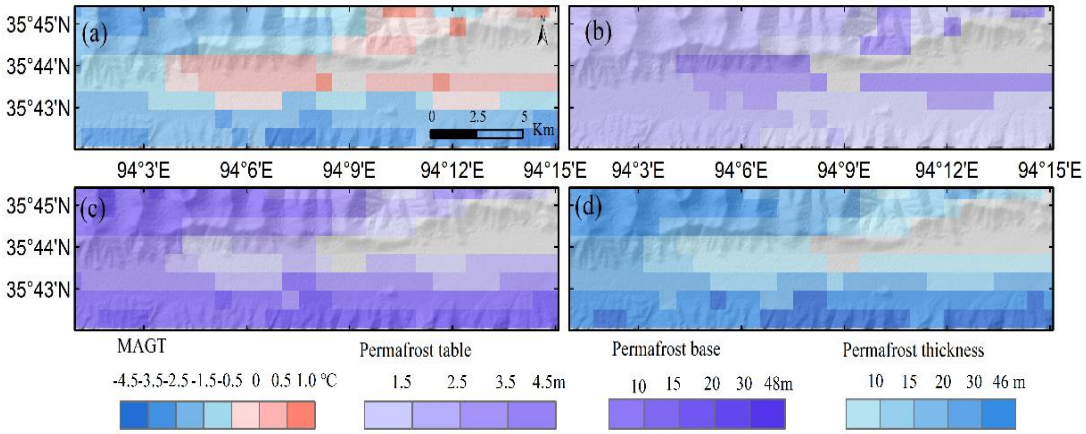

Figure 8. Spatial distributive features of MAGT (a), permafrost table (b), permafrost base (c), and permafrost thickness (d) for the initial simulation of the 1970s over the Xidatan (grey areas with the seasonally frozen ground were excluded).

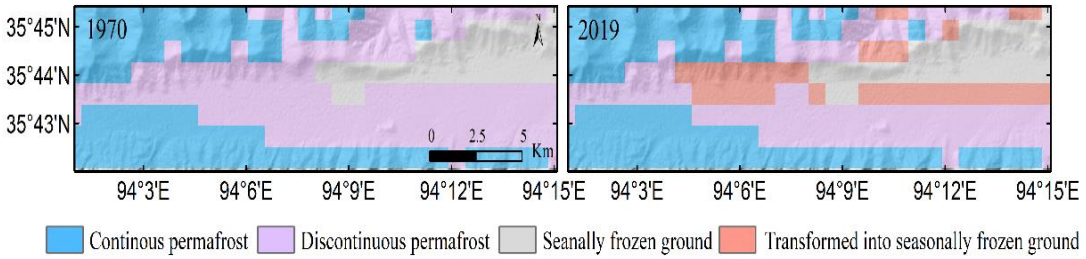

Figure 9. Spatial distributive changes of continuous and discontinuous permafrost, and seasonally frozen ground zone over the Xidatan from 1970 to 2019 (grey areas with the seasonally frozen ground were excluded).

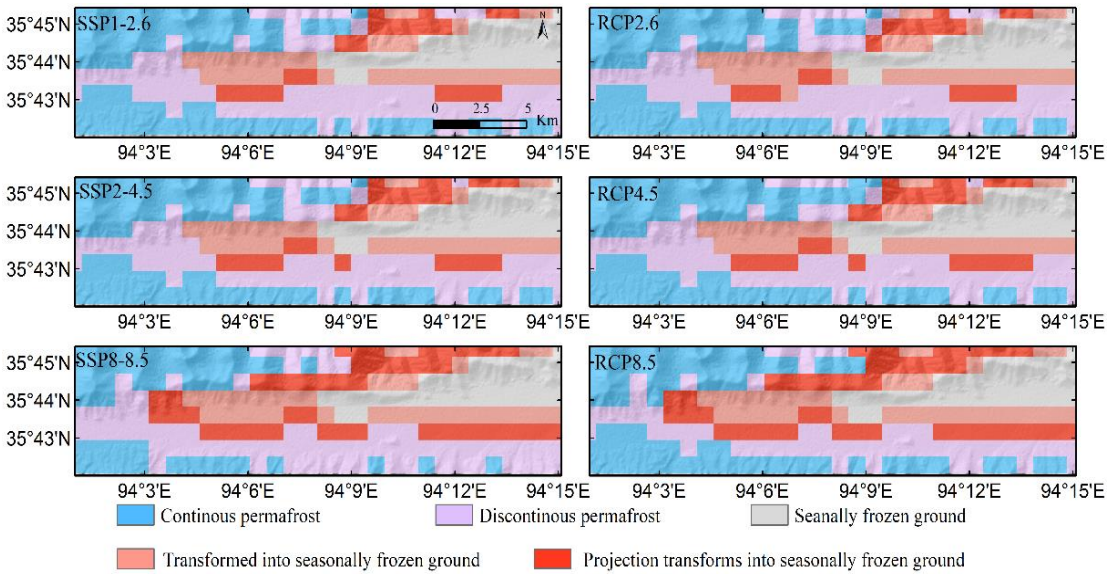

Figure 10. Projected spatial distributive changes of continuous, discontinuous, and seasonally frozen ground over the Xidatan in the future period by 2100 under RCPs and SSPs scenarios (left column, from top to bottom, each row shows under SSP1–2.6, SSP2–4.5, and SSP5–8.5 scenarios, right column, from top to bottom, each row shows under RCP2.6, RCP4.5, and RCP8.5 scenarios).

Response to Reviewer#2

Review of "Simulation of the current and future dynamics of permafrost near the northern limit of permafrost on the Qinghai–Tibet Plateau" By Zhao et al.

Climate warming has undoubtedly impacted the Cryospheric over the Tibetan Plateau. As the most widely distributed cryosphere element, thawed permafrost has caused damage to the natural and social economy; therefore, projections of the permafrost dynamics are the primary step to mitigating and adapting to climate change. Aiming to understand the permafrost dynamics on the regional scale, a model is a more powerful tool than fieldwork. Here, Zhao et al. apply a one-dimension heat conduction model to detect the permafrost change located on the permafrost's northern edge over the Tibetan Plateau. After evaluating the model's performance based on borehole records, the authors investigated the permafrost dynamics under historical and future climate conditions and claimed the terrain strongly affected the thermal regime of permafrost in the Xidatan area.
In general, this work should deserve attention or consideration by The Cryosphere if the authors could address review comments and add additional information.

Response:

Thanks a lot for the comments on our paper, which helped us to improve the quality of the manuscript. Following is our detail response to those comments and describe how we addressed these our revised manuscript. The original reviewer comments are in normal black font while our answers appear in bule font. The corresponding edit in the manuscript are included in red font.

General comments:

1. It is hard for me to understand the approach that the authors applied to generate the forcing data for the future period (last paragraph of section 2.3.3). Firstly, why do authors regard the warming climate rate in the Xidatan Area as equal to the warming rate over the Tibetan Plateau in the future? In other words, why the mean warming rate of the larger area (e.g., Tibetan Plateau) can represent that of the smaller area (e.g., Xidatan area)? Secondly, if I understand the function (Eq 8 in Sun et al., 2019) which calculates the daily land surface temperature correctly, why do the authors consider the forcing data (land surface temperature) is linearly increasing in the future? Perhaps, the results of future projections in this manuscript may overestimate the permafrost degradation conditions in the future.

Response:

We share the reviewer's concern as well which was discussed at length by the authors during the study's design.

Firstly, considerable studies have evaluated the performance of the CMIP5/CMIP6 model in simulating temperature over the QTP during the 21st century (You et al., 2021; Lun et al., 2021; Gui et al., 2021; Zhu et al., 2020; Jia et al., 2019; Hu et al., 2014). Their results suggest that much large discrepancies and uncertainties appeared between GCM/regional climate model (RCM) historical period simulations and observed climate on the QTP due to the high and complex topography, the vagaries of the local climate environment, the sparseness of meteorological stations on the plateau (You et al., 2021; Su et al., 2013; Chen et al., 2017). There is a problem that historical climate simulations are not reliable and how to accurately estimate future projections. Furthermore, overly coarse model resolution (typically on the order of several degrees of latitude/ longitude or coarser spatial resolution) capture the more detailed regional information which has been identified as important in determining the QTP climatology (Zhu et al.,2013; Gao et al., 2008). Moreover, these coarse resolutions are difficult to match well, and are not suitable for regional or smaller scales permafrost and climate change assessment. Therefore, an adaptation of results from GCM/RCM runs to the small-area and marginal permafrost, like Xidatan, is highly problematic, which leads to an inaccurate projection of permafrost. The primary objective of this study was realistically simulation the distribution of marginal permafrost on the QTP, thereby quantitatively assess historical (1970-2019) evolution process of mountain permafrost in the northern lower limit of the permafrost zone (Xidatan) on the QTP. Our model is validated at several sites throughout Xidatan against observations, we consistently reproduced the vertical ground temperature profile and active layer thickness for the last 10 years, and are superior in recognizing permafrost boundaries, and the present permafrost distribution is reproduced when simulating the evolution since 1970. This gives us confidence that our simulation results can capture the dominating process of heat transfer in permafrost and accurately reflect the lagging response of permafrost to climate change. Although, we anticipated the possible fate of permafrost over our study area by 2100 under RCP and SSP scenarios, and these scenarios are an area-mean warming rate of QTP and are derived from the latest IPCC AR6 evaluations (IPCC, 2021; Iturbide ET AL., 2020). We believe our simulation results can provide a relatively reasonable projection of the permafrost degradation levels over whole permafrost on the QTP under the different climate change scenarios in the foreseeable future. Unquestionable, reasonable, and high-quality air temperature projection is a need for a more credible projection of permafrost degradation. In future modeling efforts, high-resolution climate models and improved numerical representations of atmospheric circulation systems and land-atmosphere interactions over the heterogeneous QTP region could be one of the crucial steps toward improving the accuracy of permafrost degradation projections.

Secondly, the near-surface ground temperature is greatly affected by seasonal variations in air temperatures, characteristic of frequent fluctuations and complex patterns of variation (Lunardini et al., 1995). In the permafrost region, coupling among environmental conditions, thermal properties, phase change, ground ice, and cryoturbation make the amplitude of the seasonal cycle increasingly attenuate with depth until approaching undetectable temperature variation at a depth of annual zero amplitude. (Less than instrument measurable accuracy, generally with the range of 0.1°C, and at 10–20 m on the QTP) (Jin et al., 2011; Dobiński, et al., 2022). Such that the ground is a natural low-pass filter of the short-term meteorological signal. Decadal or longer time-scale climate variations trend (the ‘signal’), however, can penetrate to deeper permafrost and hence be retained, which records past temperature changes at the ground surface (Romanovsky, 2010; Biskaborn,2019). Thus,

the variations trend of mean annual ground temperature at the depths of zero annual amplitude is generally consistent with the long-term trend of air temperature while the distribution of warming during the year has little effect on long-term permafrost degradation (Smith and Riseborough, 1983; Buteau et al., 2004; Biskaborn,2019). As mentioned above, here, the focus of this study is to discuss the long-term trend of the permafrost temperature over the foreseeable future. Because of a linearly warming trend is projected in mean annual air temperature over the QTP during the 21st century under different climate change scenarios, and a strong linear relationship between GST and AT over our study area. Hence, forcing data (land surface temperature) to increase linearly in the future in our work cannot affect the long-term variations trend of permafrost temperature.

In the revised manuscript, we have made a supplement to the description of the current limitation in projection of permafrost degradation and future improvements in the discussion section. The text there reads as: "*The limitation of this study includes that projected the possible fate of permafrost over Xidatan by 2100, under an area-mean warming rate scenario of QTP. Hence, the anticipated permafrost degradation in this study, may not be the actual overview, as it does not consider the regional-level or small-scale-based future climate change, but our simulation results can provide a relatively reasonable projection indication of the permafrost degradation levels over marginal permafrost on the QTP under the different climate change scenarios in the foreseeable future. High-resolution climate models and improved numerical representations of atmospheric circulation systems and land-atmosphere interactions over the heterogeneous QTP region could be a crucial step toward improving the GCMs/RCMs performance, thereby accuracy in the projection of permafrost degradation in the future.*"

Reference:

Lun, Y., Liu, L., Cheng, L., Li, X., Li, H., and Xu, Z.: Assessment of GCMs simulation performance for precipitation and temperature from CMIP5 to CMIP6 over the Tibetan Plateau, Int J Climatol. 41: 3994–4018. https://doi.org/10.1002/joc.7055,2021.

Cui, T., Li, C., and Tian, F.: Evaluation of temperature and precipitation simulations in CMIP6 models over the Tibetan Plateau, Earth and Space Science, 8, e2020EA001620. https://doi.org/10.1029/2020EA001620, 2021.

You, Q., Cai, Z., Wu, F., Jiang, Zhi., Pepin, N., and Shen, S.: Temperature dataset of CMIP6 models over China: evaluation, trend and uncertainty, Clim Dyn 57, 17–35https://doi.org/10.1007/s00382-021-05691-2, 2021.

Zhu, Y., and Yang, S.: Evaluation of CMIP6 for historical temperature and precipitation over the Tibetan Plateau and its comparison with CMIP5, Adv Clim Chang Res 11, 239–251, https:// doi. org/10. 1016/j. accre. 2020. 08. 001, 2020.

Jia, K., Rua, Y., Yang, Y., and You, Z.: Assessment of CMIP5 GCM simulation performance for temperature projection in the Tibetan Plateau, Earth and Space Science, 6, 2362-2378. https://doi.org/10.1029/2019EA000962, 2019.

Chen, X., Liu, Y., and Wu, G., Understanding the surface temperature cold bias in CMIP5 AGCMs

over the Tibetan Plateau, Adv. Atmos. Sci. 34, 1447-1460, https://doi.org/10.1007/s00376-017-6326-9, 2017.

Hu, Q., Jiang, D., and Fan. G.: Evaluation of CMIP5 models over the Qinghai-Tibetan Plateau, Chin. J. Atmos. Sci, 38: 924-938, 2014.

Su, F., Duan, X., Chen, D., Hao, Z., and Cuo, L.: Evaluation of the global climate models in the CMIP5 over the Tibetan Plateau. J. Climate, 26, 3187–3208, https://doi.org/10.1175/JCLI-D-12-00321.1, 2013.

Zhu, X., Wang, W., and Fraedrich, K.: Future climate in the Tibetan Plateau from a statistical regional climate model, J. Climate, 26, 10125-10138, https://doi.org/10.1175/JCLI-D-13-00187.1, 2013.

Gao, X., Shi, Y., Song, R., Giorgi, F., Wang, Y., and Zhang, D.: Reduction of future monsoon precipitation over China: Comparison between a high-resolution RCM simulation and the driving GCM, Meteorol. Atmos. Phys., 100, 73–86, doi:10.1007/s00703-008-0296-5, 2008.

Lunardini, V.: Permafrost Formation Time. CRREL Report 95-8, US Army Corps of Engineers, Cold Regions Research and Engineering Laboratory, 1995.

Dobiński, W., and Marek K.: Permafrost Base Degradation: Characteristics and Unknown Thread With Specific Example From Hornsund, Svalbard, Front. Earth Sci. 10:802157, doi: 10.3389/feart.2022.802157, 2022.

Romanovsky, V., Oberman, N., Drozdov, D., Malkova, G., Kholodov, A., and Marchenko, S.: Permafrost, in Changes in the Arctic: Background and Issues, 80-82, 2010.

Iturbide, M., Gutiérrez, J., Alves, L., Bedia, J., Cerezo-Mota, R., Cimadevilla, E., Cofiño, A., Di, L., Faria, S., Gorodetskaya, I., Hauser, M., Herrera, S., Hennessy, K., Hewitt, H., Jones, R., Krakovska, S., Manzanas, R., Martínez-Castro, D., Narisma, G., Nurhati, I., Pinto, I., Seneviratne, S., van den Hurk, B., and Vera, C.: An update of IPCC climate reference regions for subcontinental analysis of climate model data: definition and aggregated datasets, Earth Syst. Sci. Data, 12, 2959–2970, https://doi.org/10.5194/essd-12-2959-2020,2020

IPCC. Climate change 2021: the physical science basis, https://www.ipcc.ch/report/ar6/wg1/downloads/report/IPCC_AR6_WGI_Full_Report.pdf., 2021.

Noetzli, J., Matthes, H., Vieira, G., Streletskiy, D., Schoeneich, P., Romanovsky, V., Lewkowicz, A., Abramov, A., Allard, M., Boike, J., Cable, W., Christiansen, H., Delaloye, R., Diekmann, B., Drozdov, D., Etzelmüller, B., Grosse, G., Guglielmin, M., Ingeman-Nielsen, T., Isaksen, K., Ishikawa, M., Johansson, M., Johannsson, H., Joo, A., Kaverin, D., Kholodov, A., Konstantinov, P., Kröger, T., Lambiel, C., Lanckman, J., Luo, D., Malkova, G., Meiklejohn, I., Moskalenko, N., Oliva, M., Phillips, M., Ramos, M., Sannel, A., Sergeev, d., Seybold, C., Skryabin, P., Vasiliev, A., Wu, Q., Yoshikawa, K., Zheleznyak, M., Lantuit, H.: Permafrost is warming at a global scale. Nat Commun 10, 264, https://doi.org/10.1038/s41467-018-08240-4, 2019.

Smith, M., Riseborough, D.: Permafrost sensitivity to climatic change. In Proceedings, 4th International Conference on Permafrost, Vol. 1. Fairbanks, Alaska, National Academy Press: Washington, DC; 1178–1183, 1983.

Buteau, S., Fortier, R., Delisle, G., and Allard, M.: Numerical simulation of the impacts of climate warming on a permafrost mound, Permafrost and Periglac. Process., 15, 41-57, https://doi.org/10.1002/ppp.474, 2004.

Jin, H., Luo, D., Wang, S., Lü, L., and Wu, J.: Spatiotemporal variability of permafrost degradation on the Qinghai-Tibet Plateau, Sci. Cold Arid Reg., 3, 281–305, DOI: 10.3724/SP.J.1226.2011.00281, 2011.

2. For the methods of spatially modeling (Section 2.3.4), how the authors obtain the soil stratigraphy in the area without any borehole, e.g., 35°40' N - 35°42', because the authors pointed out that "the well-adjusted thermos-physical parameters of multilayered soil columns during the model calibration were specified and assigned for each grid cell of the same soil classes in the surrounding areas of the calibrating borehole".

Response:

In our work, the soil stratigraphy in the area without any boreholes was defined based on the surficial soil type maps at 1km × 1km spatial resolution. The map is mainly based on the relationships between environmental factors and soil types in the permafrost region of the QTP by applying a decision-making tree to spatialize the soil types (Li et al., 2014, 2015b). The results exhibited good reliability and thus could be used to realize the spatialization of soil thermal properties (Zou et al., 2017). The horizontal resolution of the simulation was 1km×1km, and the model domain ranged from 35°42′N to 35°45′N and from 94°3′E to 94°15′E, and encompasses an area of 280 km^2.We collected as many as fifteen monitoring boreholes with long-term temperature observation established in the Xidatan, which were specific for each soil type class and geographical location. Thermophysical properties (e.g., stratigraphies, texture, ground ice content, organic matter content, dry bulk density) of distinct soil layers were measured or assessed for field surveys, laboratory, and on-site measurement, as well as tests on soil samples obtained from fifteen borehole cores (depth between 8~30 m). Based on these properties, we calibration thermophysical parameters of different soil layers, then, well–adjusted thermos–physical parameters of multilayered soil columns were assigned for each soil type for spatial modeling.

To be clear, we have stated in the revised manuscript that *"Based on the soil type map at 1km×1km spatial resolution, well–adjusted thermos–physical parameters of multilayered soil columns in section 2.3.2 were specified and assigned for each soil type."*

Reference:

Li, W., Zhao, L., Wu, X., Zhao, Y., Fang, H., and Shi, W.: Distribution of soils and landform relationships in the permafrost regions of Qinghai-Xizang (Tibetan) Plateau, Chinese Sci. Bull., 60, 2216–2226, https://doi.org/10.1360/N972014-01206, 2015b.

Zou, D., Zhao, L., Sheng, Y., Chen, J., Hu, G., Wu, T., Wu, J., Xie, C., Wu, X., Pang, Q., Wang, W., Du, E., Li, W., Liu, G., Li, J., Qin, Y., Qiao, Y., Wang, Z., Shi, J., and Cheng, G.: A new map of permafrost distribution on the Tibetan Plateau, The Cryosphere, 11, 2527–2542, https://doi.org/10.5194/tc-11-2527-2017, 2017.

3. I suggested the authors should be better replot Fig 2-5, because it is hard for me to see the model's performance.

Response:

We have replotted Fig. 2-5 to make the contrast clearer, and shown as follows.

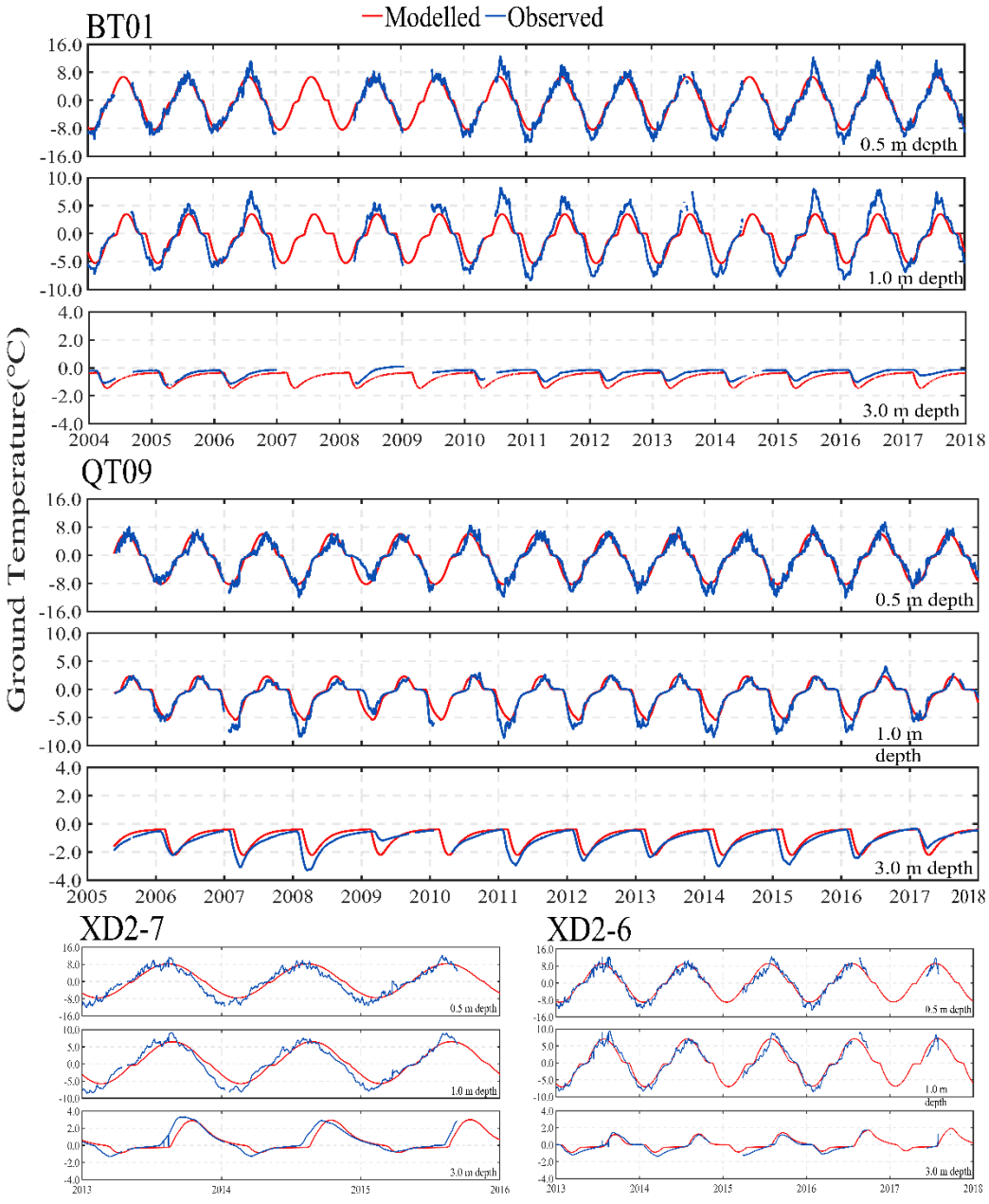

Figure 2. Comparison of the modelled (red lines) to observed (blue lines) daily mean ground temperature at 0.5

m, 1.0 m, 3.0 m depth in four calibration boreholes (BT01, XD2-7, QT09, and XD2-6) during the observation period (There were some data gaps due to temperature probe failure in some years, at the BT01, the data gaps in the record mainly occurred at 0.5-15 m in 2007-2008, and at 15-30 m during the 2005-2007 and 2011-2018, at the QT09, observations at 15-30 m of 2006-2008, 2011-2013, and 2015-2018 are not available, at the XD2-6, the data gap in the record in 2016-2017).

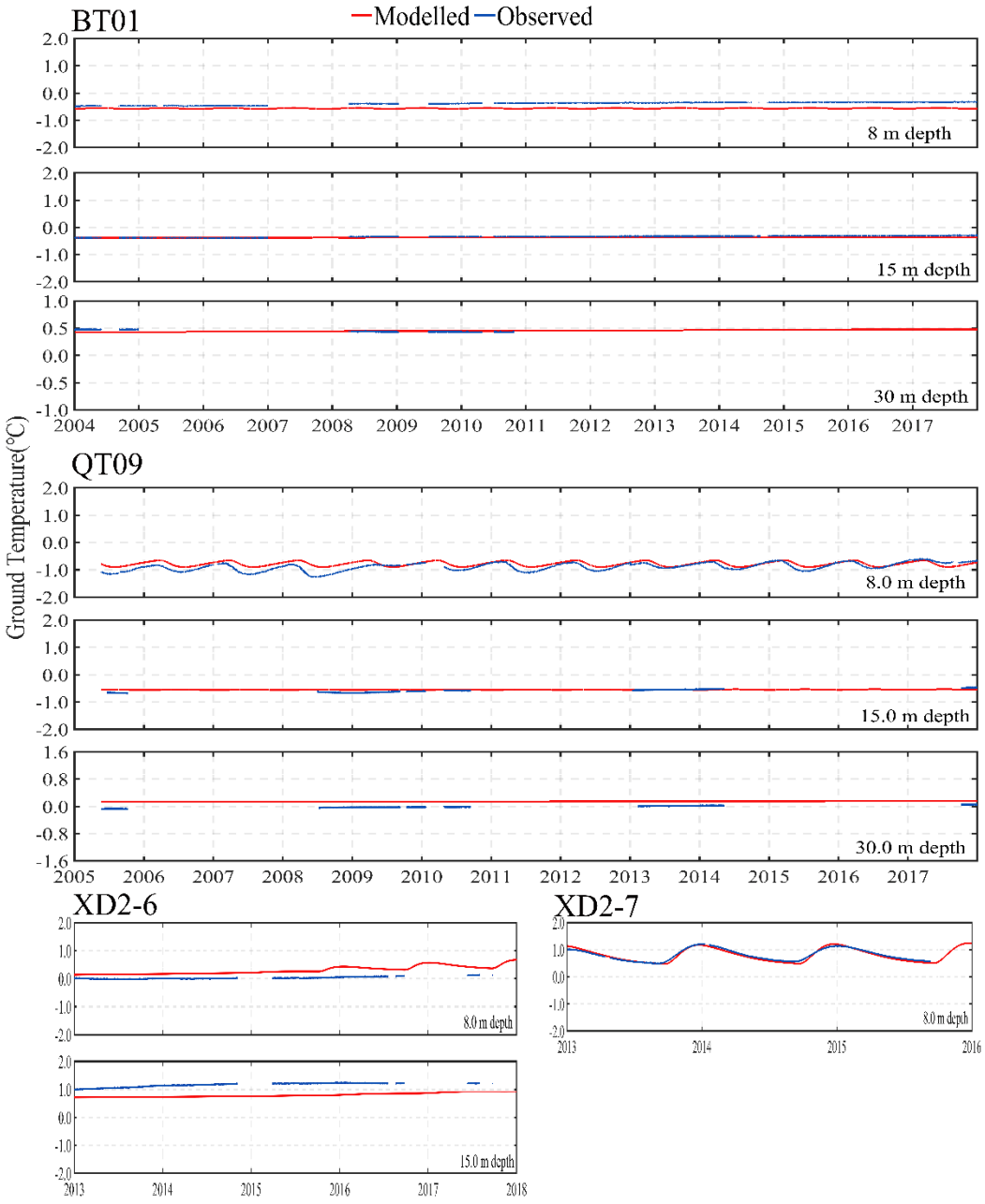

Figure 3. Same as Figure 2. but for daily mean ground temperature at 8 m, 15 m, and 30 m.

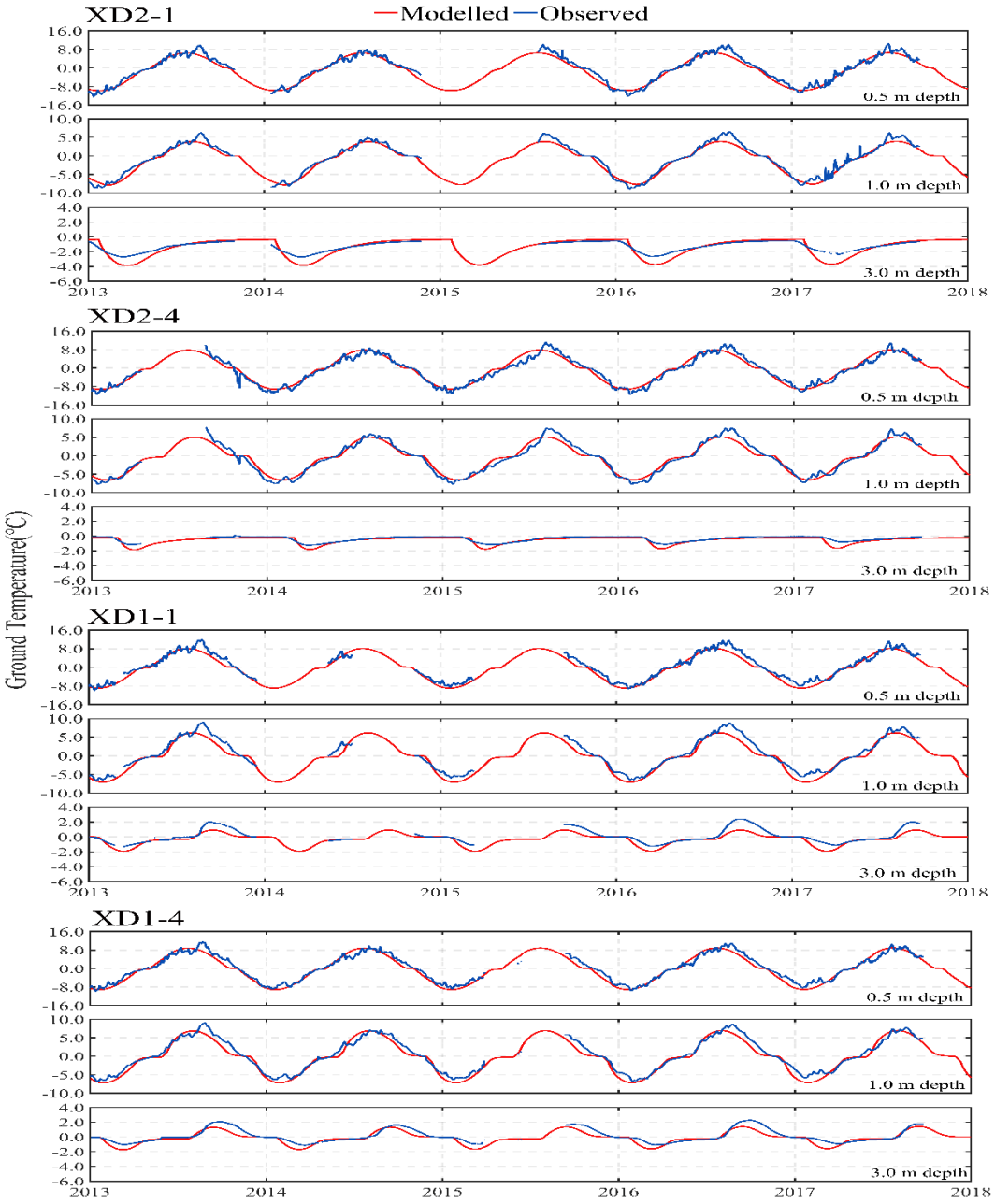

Figure 4. Comparison of the simulated (red lines) to observed (blue lines) daily mean ground temperature at 0.5 m, 1.0 m, and 3.0 m depth in four validation boreholes (XD2-1, XD2-4, XD1-1, and XD1-4) during the observation period from 2013 to 2018 (There were some data gaps due to temperature probe failure in some years, at the XD2-1, the data gaps in the record mainly occurred at 0.5-3.0 m in the first half of 2015. At the XD1-1, the data gap in the record at 0.5-3.0 in 2014-2015, at 8-15 m during the 2013-2015. At the XD1-4, the data gap in the record in the first half of 2015).

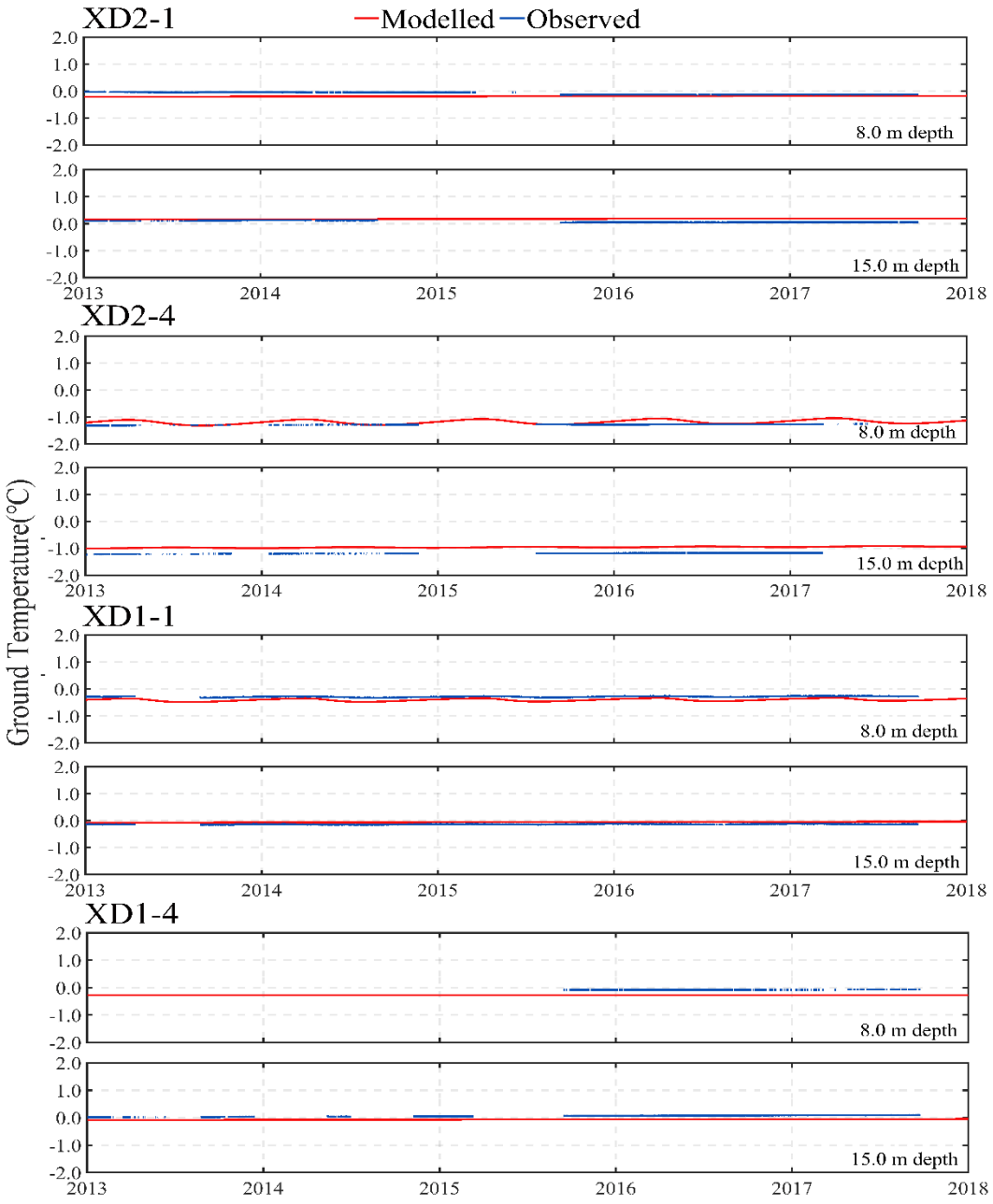

Figure 5. Same as Figure 4. But for daily mean ground temperature at 8 m, and 15 m.

4. For the third paragraph of section 4.2, the authors cited some projection studies that used statistical methods to detect the permafrost state in the future. But, as far as I know, there are existed some studies using the land surface model to simulate the permafrost change over the Tibetan Plateau, e.g., Guo et al., (2012), Qin et al., (2017), and Zhang et al., (2022). Therefore, what is the advantage of the model used in this manuscript compared to other numerical transient models?

Response:

Thank you very much for the literature, we read it carefully.

Qin et al. (2012) also used the one-dimensional heat conduction permafrost model (GIPL) modeling of the active layer thickness and permafrost thermal state across QTP. But it does not consider ground thermal dynamics and is for equilibrium conditions, and no projection. By contrast, our simulation integrated climate and ground condition variables to quantify the change in permafrost under current and future climate change.

For Land Surface Lands (LSMs), Guo et al. (2012) used the Community Land Model4 (CLM4) to project that an approximately 81% reduction in near surface (<4.5 m) permafrost area on the QTP by the end of the 21st century under the A1B emission scenario. Additionally, the deep permafrost depths of 10 and 30m would be largely degraded by the year 2030-2050. Zhang et al. (2022) applied Noah LSM to project much of 44 ± 4%, 59 ± 5%, and 71 ± 7%, the permafrost is likely to degrade in the late 21st century, under SSP2-4.5, SSP3-7.0, and SSP5-8.5 scenarios, respectively, by 2100. These results and our simulation results unanimously revealed that further permafrost degradation tend was projected over the QTP under warm scenarios, but with a considerable discrepancy among these results on the magnitude of permafrost degradation. This discrepancy can, in part, be attributed to deficits of LSMs. Most of those LSMs were originally developed for shallow soil simulation, and the subsequent studies mainly focused on optimizing parameterization schemes and simply extending the soil column simulation depth, but they were poor with regard to considering the effecting of ground ice, thermal state of deep permafrost and geothermal heat flux (Sun et al. 2019, Lee et al., 2014). For example, ignoring the geothermal heat flux by setting zero flux or constant temperature as the bottom boundary condition (Wu et al., 2010; Xiao et al., 2013). However, these factors play a crucial role in the long-term evolution of permafrost in general (Xiao et al., 2013; Wu et al., 2010; Lee et al., 2014). Thus, the relationship between the decrease in the areal extent of permafrost and the warming air temperature over the present-day permafrost region is approximately linear simulated by LSMs. Given that such high rates of permafrost loss are not observed, this indicates a too-high sensitivity for those models predicting such losses (Zhao et al., 2020).

In comparison, our model considers the thermal property difference between frozen and thawed soil, the phase variations of the unfrozen water in frozen soil, the distribution of the ground ice, and geothermal heat flow. Thereby, can well describe the heat transfer process in permafrost and reasonably capture the attenuation and time lag of heat transfer in deep permafrost as water or ice content and ground is a poor conductor of heat. Moreover, our model is characterized by vertical modeling domains of one hundred meters with a vertical resolution of 0.05m within the active layer (the upper 4 m) and provides sufficient accuracy to resolve the annual dynamics of active layer thawing and refreezing, as well as the evolution of ground temperature in deeper layers. Our simulation results were reasonable and in compliance with observed facts. Moreover, the magnitude and evolution of permafrost degradation projection on the QTP derived our transient simulations agree well with that of the heat conduction permafrost model account for the thermal state of deep ground ice (Li et al., 1996; Li et al., 2008; Sun et al., 2019). It can be noted that existing LSMs simulations largely ignore the thermal properties of deep permafrost, but our findings highlight initial permafrost thermal state is influenced by historical climate, stratigraphy thermal properties, ground ice distribution, geothermal heat flow, and propagation of the phase-transition interface plays a critical role in permafrost degradation.

In the revised manuscript, we have added a discussion about what is the advantage of the model used in this manuscript compared to other numerical transient models (e.g., LSMs) in section 4.2. these studies have been cited in the revised manuscript as follows. *"For Land Surface Lands (LSMs), Guo et al. (2012) used the Community Land Model4 (CLM4) to projects that an approximately 81% reduction in near surface (<4.5 m) permafrost area on the QTP by the end of the 21st century under the A1B emission scenario. Additionally, the deep permafrost depths of 10 and 30m would be largely degraded by the year 2030-2050. Zhang et al. (2022) applied Noah LSM to project much of 44 ± 4%, 59 ± 5%, and 71 ± 7%, the permafrost is likely to degrade in the late 21st century, under SSP2-4.5, SSP3-7.0, and SSP5-8.5 scenarios, respectively, by 2100."*

Reference

Qin, Y., Wu, T., Zhao, L., et al. 2017. Numerical modeling of the active layer thickness and permafrost thermal state across Qinghai-Tibetan Plateau. 122, 11604-11620. Journal of Geophysical Research: Atmospheres. https://doi.org/10.1002/2017JD026858.

Guo, D., Wang, H., Li, D. 2012. A projection of permafrost degradation on the Tibetan Plateau during the 21st century. 117, D05106. Journal of Geophysical Research: Atmospheres. https://doi.org/10.1029/2011JD016545.

Zhang, G., Nan, Z., Hu, N., et al. 2022. Qinghai-Tibet Plateau permafrost at risk in the late 21st Century. Earth's Future. 10, e2022EF002652. https://doi.org/10.1029/2022EF002652.

Sun, Z., Zhao, L., Hu, G., Qiao, Y., Du, E., Zou, D., Xie, C.: Modeling permafrost changes on the Qinghai-Tibetan plateau from 1966 to 2100: a case study from two boreholes along the Qinghai-Tibet engineering corridor. Permafrost and Periglac. Process., 32:156-171, https://doi.org/10.1002/ppp.2022, 2019.

Zhao, L., Zou, D. Hu, G., Du, E., Pang, Q., Xiao, Y., Li, R., Sheng, Y., Wu, X., Sun, Z., Wang, L., Wang, C., Ma, L., Zhou, H., and Liu, S.: Changing climate and the permafrost environment on the Qinghai–Tibet (Xizang) Plateau, Permafrost Periglac., 31, 396–405, https://doi.org/10.1002/ppp.2056, 2020.

Wu, Q., Zhang, T., and Liu, Y.: Permafrost temperatures and thickness on the Qinghai-Tibet Plateau, Global Planet. Change., 72, 32-38, https://doi.org/10.1016/j.gloplacha.2010.03.001, 2010.

Xiao, Y., Zhao, L., Dai, A., Li, R., Pang, Q., Yao, J.: Representing permafrost properties in CoLM for the Qinghai–Xizang (Tibetan) Plateau, 87, 68-77, https://doi.org/10.1016/j.coldregions.2012.12.004, 2013.

Hanna Lee, H., Swenson, S., Slater, A., and Lawrence, D.: Effects of excess ground ice on projections of permafrost in a warming climate, Environ. Res. Lett. 9 124006, doi:10.1088/1748-9326/9/12/124006, 2014.

Li, S., Cheng, G., and Guo, D.: The future thermal regime of numerical simulating permafrost on the Qinghai-Xizang (Tibet) Plateau, China, under a warming climate. Science in China, Ser. D, 434-441,1996.

Li, D., Chen, J., Meng, Q., Liu, D., Fang, J., and Liu, J.: Numeric simulation of permafrost degradation in the eastern Tibetan Plateau, Permafrost and Periglac. Process., 19, 93-99, https://doi.org/10.1002/ppp.611,2008.

Specific comments

1. I do not see any citations for Table 2 and Table 3 in the manuscript.

Response:

The values of the thermal conductivity and heat capacity were from:

Yershov, E.: Principles of Geocryology (in Chinese), Lanzhou University Press, Lanzhou, China, 2016 (pp. 207-215).

Construction Ministry of PRC.: Code for design of soil and foundation of building in frozen soil region (in Chinese), China Architecture and Building Press, Beijing, China, 2011 (pp. 86-91), S86-S91.

工程建设标准全文信息系统

附录K　冻土、未冻土热物理指标的计算(值)

K.0.1　根据土的类别、天然含水量及干密度测定数值，冻土和未冻土的容积热容量、导热系数和导温系数可分别按表K.0.1-1～表K.0.1-4取值。大含水(冰)量土的导热系数在无实测资料时可按表K.0.1-5取值。

草炭粉质粘土计算热参数值　　表K.0.1-1

ρ_d (kg/m³)	w (%)	C_u (kJ/m³·℃)	C_f (kJ/m³·℃)	λ_u (W/m·℃)	λ_f (W/m·℃)	$a_u \cdot 10^3$ (m²/h)	$a_f \cdot 10^3$ (m²/h)
400	30	903.3	710.9	0.13	0.13	0.50	0.62
	50	1237.9	878.2	0.19	0.22	0.52	0.92
	70	1572.4	1045.5	0.23	0.37	0.54	1.26
	90	1907.0	1212.8	0.29	0.53	0.56	1.59
	110	2241.6	1380.1	0.35	0.72	0.57	1.87
	130	2576.1	1547.3	0.41	0.88	0.57	2.06
500	30	1129.1	890.8	0.17	0.17	0.54	0.69
	50	1547.3	1099.9	0.24	0.31	0.56	1.30
	70	1965.5	1309.0	0.32	0.51	0.59	1.40
	90	2383.7	1518.1	0.41	0.74	0.61	1.76
	110	2801.9	1727.2	0.49	1.00	0.62	2.08
	130	3220.0	1936.3	0.56	1.24	0.63	2.31
600	30	1355.0	1066.4	0.22	0.22	0.57	0.76
	50	1856.8	1317.3	0.31	0.42	0.61	1.15
	70	2358.5	1568.3	0.42	0.68	0.64	1.56
	90	2860.5	1819.2	0.53	0.99	0.67	1.95
	110	3362.3	2070.1	0.63	1.32	0.68	2.29
	130	3864.2	2321.0	0.75	1.61	0.68	2.51

工程建设标准全文信息系统

工程建设标准全文信息系统

续表

ρ_g (kg/m³)	w (%)	C_u (kJ/m³·℃)	C_f (kJ/m³·℃)	λ_u (W/m·℃)	λ_f (W/m·℃)	$\alpha_u \cdot 10^3$ (m²/h)	$\alpha_f \cdot 10^3$ (m²/h)
700	30	1580.8	1246.2	0.27	0.30	0.61	0.87
	50	2166.3	1539.0	0.39	0.56	0.65	1.30
	70	2375.4	1831.7	0.53	0.88	0.70	1.74
	90	3337.2	2124.5	0.66	1.26	0.71	2.14
	110	3922.7	2417.2	0.79	1.67	0.73	2.50
	130	4508.2	2709.9	0.92	2.01	0.73	2.77
800	30	1806.6	1421.9	0.32	0.37	0.65	0.94
	50	2475.7	1756.4	0.48	0.68	0.70	1.41
	70	3144.9	2091.0	0.64	1.09	0.73	1.67
	90	3814.0	2425.6	0.80	1.55	0.78	2.32
	110	4483.1	2760.1	0.96	2.05	0.77	2.68
	130	5152.2	3094.7	1.10	2.47	0.78	2.88
900	30	1171.0	1342.4	0.38	0.40	0.68	1.03
	50	2785.2	1978.1	0.57	0.73	0.73	1.53
	70	3538.0	2354.5	0.75	1.14	0.77	2.03
	90	4290.7	2370.8	0.95	1.63	0.80	2.49
	100	5043.5	3107.2	1.14	2.12	0.82	2.86
	130	5796.3	3483.6	1.32	2.52	0.82	3.02

注：① 表中符号：ρ_g—干密度；w—含水量；λ—导热系数；C—容积热容量；α—导温系数；脚标：u—未冻土，f—已冻土。下同；

②表列数值可直线内插。

粉土、粉质粘土计算热参数值　　表 K.0.1-2

ρ_g (kg/m³)	w (%)	C_u (kJ/m³·℃)	C_f (kJ/m³·℃)	λ_u (W/m·℃)	λ_f (W/m·℃)	$\alpha_u \cdot 10^3$ (m²/h)	$\alpha_f \cdot 10^3$ (m²/h)
1200	5	1254.6	1179.3	0.25	0.26	0.73	0.76
	10	1505.5	1405.2	0.43	0.41	1.02	1.04
	15	1756.4	1530.6	0.58	0.58	1.19	1.37
	20	2007.4	1656.1	0.67	0.79	1.21	1.71
	25	2258.3	1781.5	0.72	1.04	1.14	2.10
	30	2509.2	1907.0	0.79	1.28	1.13	2.40
	35	2760.1	2032.5	0.86	1.45	1.12	2.57

工程建设标准全文信息系统

工程建设标准全文信息系统

续表

ρ_g (kg/m³)	w (%)	C_u (kJ/m³·℃)	C_f (kJ/m³·℃)	λ_u (W/m·℃)	λ_f (W/m·℃)	$\alpha_u \cdot 10^3$ (m²/h)	$\alpha_f \cdot 10^3$ (m²/h)
1300	5	1359.2	1279.7	0.30	0.29	0.80	0.80
	10	1631.0	1522.2	0.50	0.48	1.11	1.12
	15	1902.8	1660.3	0.71	0.71	1.33	1.47
	20	2174.6	1794.1	0.79	0.92	1.31	1.85
	25	2446.5	1932.1	0.84	1.21	1.23	2.25
	30	2718.3	2065.9	0.90	1.46	1.19	2.55
	35	2990.1	2203.9	0.97	1.67	1.18	2.74
1400	5	1463.7	1375.9	0.36	0.35	0.87	0.90
	10	1756.4	1539.3	0.59	0.57	1.22	1.22
	15	2049.2	1785.7	0.84	0.79	1.46	1.58
	20	2341.9	1932.1	0.94	1.06	1.44	1.96
	25	2634.7	2496.7	0.97	1.39	1.33	2.41
	30	2927.4	2224.8	1.06	1.68	1.32	2.73
	35	3220.1	2371.2	1.18	1.93	1.32	2.92
1500	5	1568.3	1476.2	0.41	0.41	0.93	0.98
	10	1881.9	1756.4	0.67	0.65	1.28	1.32
	15	2191.4	1907.0	0.96	0.91	1.58	1.71
	20	2509.2	2070.1	1.09	1.22	1.57	2.12
	25	2822.9	2229.0	1.13	1.58	1.44	2.55
	30	3136.5	2383.7	1.24	1.89	1.43	2.85
	35	3450.2	2542.7	1.36	2.12	1.42	3.01
1600	5	1672.8	1572.4	0.46	0.46	1.01	1.05
	10	2425.6	1873.5	0.78	0.74	1.40	1.42
	15	2541.9	2040.8	1.11	1.02	1.72	1.81
	20	2676.5	2208.1	1.24	1.38	1.67	2.25
	25	3011.0	2375.4	1.28	1.80	1.52	2.73
	30	3345.6	2542.7	1.42	2.12	1.52	3.01
	35	3680.2	2709.9	1.54	2.40	1.51	3.20

工程建设标准全文信息系统

工程建设标准全文信息系统

碎石粉质粘土计算热参数值　　表 K.0.1-3

ρ_d (kg/m³)	w (%)	C_u (kJ/m³·℃)	C_f (kJ/m³·℃)	λ_u (W/m·℃)	λ_f (W/m·℃)	$\alpha_u \cdot 10^3$ (m²/h)	$\alpha_f \cdot 10^3$ (m²/h)
1200	3	1154.2	1053.9	0.23	0.22	0.72	0.77
	7	1355.0	1154.2	0.34	0.37	0.91	1.15
	10	1505.5	1229.5	0.43	0.52	1.03	1.52
	13	1656.1	1304.8	0.53	0.71	1.16	1.96
	15	1756.4	1355.0	0.59	0.85	1.21	2.26
	17	1856.8	1405.2	0.60	0.94	1.26	2.42
1400	3	1346.6	1229.5	0.34	0.32	0.89	0.97
	7	1568.3	1346.6	0.50	0.53	1.15	1.44
	10	1756.4	1434.4	0.65	0.74	1.33	1.86
	13	1932.1	1522.2	0.79	0.97	1.48	2.30
	15	2049.2	1580.8	0.88	1.14	1.55	2.59
	17	2166.3	1639.3	0.92	1.24	1.53	2.73
1600	3	1539.0	1405.2	0.46	0.45	1.07	1.17
	7	1806.6	1539.0	0.68	0.74	1.38	1.73
	10	2007.4	1639.3	0.89	1.00	1.61	2.20
	13	2208.1	1739.7	1.10	1.29	1.80	2.66
	15	2341.9	1806.6	1.28	1.45	1.87	2.90
	17	2475.7	1873.5	1.42	1.57	1.96	3.02
1800	3	1731.3	1580.8	0.60	0.60	1.25	2.38
	7	2032.5	1731.3	0.92	0.97	1.62	2.43
	10	2258.3	1844.3	1.17	1.31	1.87	2.58
	13	2295.9	1957.2	1.45	1.65	2.10	3.03
	15	2634.7	2032.5	1.60	1.82	2.19	3.23
	17	2785.2	2107.7	1.71	1.93	2.21	3.28

工程建设标准全文信息系统

工程建设标准全文信息系统

砾砂计算热参数值　　表 K.0.1-4

ρ_d (kg/m³)	w (%)	C_u (kJ/m³·℃)	C_f (kJ/m³·℃)	λ_u (W/m·℃)	λ_f (W/m·℃)	$\alpha_u \cdot 10^3$ (m²/h)	$\alpha_f \cdot 10^3$ (m²/h)
1400	2	1229.5	1083.1	0.42	0.49	1.23	1.62
	6	1463.7	1200.2	0.96	1.14	2.36	3.42
	10	1697.9	1317.3	1.17	1.43	2.40	3.91
	14	1932.1	1434.4	1.29	1.67	2.40	4.20
	18	2166.3	1551.5	1.39	1.86	2.27	4.31
1500	2	1317.3	1162.6	0.50	0.59	1.36	1.84
	6	1568.3	1288.1	1.09	1.32	2.51	3.70
	10	1819.2	1413.5	1.30	1.60	2.58	4.08
	14	2070.1	1539.0	1.44	1.87	2.51	4.38
	18	2321.0	1664.4	1.52	2.08	2.37	4.50
1600	2	1405.2	1237.9	0.61	0.73	1.56	2.13
	6	1672.8	1371.7	1.28	1.60	1.74	4.21
	10	1940.4	1505.5	1.48	1.86	2.75	4.44
	14	2208.1	1639.3	1.64	2.15	2.67	4.72
	18	4173.6	1773.2	1.69	2.35	2.47	4.79
1700	2	1493.0	1317.3	0.77	0.94	1.85	2.52
	6	1777.4	1459.5	1.47	1.91	2.99	4.73
	10	2061.7	1601.7	1.68	2.20	2.94	4.96
	14	2346.1	1743.9	1.84	2.48	2.84	5.13
	18	2630.5	1886.1	1.95	2.69	2.66	5.14
1800	2	1580.8	1392.6	0.95	1.19	2.17	3.09
	6	1881.9	1543.2	1.71	2.27	3.27	5.31
	10	2183.0	1693.7	1.91	2.61	3.17	5.56
	14	2484.1	1844.3	2.09	2.85	3.02	5.58
	18	2785.2	1994.8	2.18	3.05	2.82	5.51

工程建设标准全文信息系统

工程建设标准全文信息系统

大含水(冰)量土的导热系数　　表 K. 0. 1-5

红色粉质粘土				黄色粉土			
青海风火山				兰州			
ρ_d (kg/m³)	w (%)	λ_u (W/m·℃)	λ_f (W/m·℃)	ρ_d (kg/m³)	w (%)	λ_u (W/m·℃)	λ_f (W/m·℃)
380	202.4	0.73	2.15	400	200.0	—	2.13
680	109.2	0.94	2.06	700	100.0	—	2.08
900	78.2	1.03	1.97	1000	55.8	—	2.05
1000	60.0	1.08	1.95	1200	40.0	1.94	2.02
1100	50.0	1.08	1.95	1400	35.0	1.86	1.91
1200	44.9	1.09	1.88	1400	30.0	1.72	1.81
1200	34.3	1.09	1.67	—	—	—	—
草炭粉土				草根(皮)			
西藏两道河				西藏两道河			
ρ_d (kg/m³)	w (%)	λ_u (W/m·℃)	λ_f (W/m·℃)	ρ_d (kg/m³)	w (%)	λ_u (W/m·℃)	λ_f (W/m·℃)
100	960.0	—	1.86	100	840	—	1.62
200	428.8	—	2.16	200	400	0.68	1.86
300	300.0	—	2.25	200	300	0.57	1.32
300	284.4	—	1.98	200	250	0.46	0.86
400	180.8	—	2.03	200	200	0.39	0.65
500	143.3	—	2.06	200	150	0.27	0.46
700	138.1	—	2.13	200	100	0.23	0.26
—	—	—	—	300	250	0.65	1.65
—	—	—	—	300	180	0.45	1.07
—	—	—	—	300	150	0.41	0.93
—	—	—	—	300	130	0.36	0.68
—	—	—	—	300	110	0.36	0.57

工程建设标准全文信息系统

2. L322-323: 0.032℃ a-1 (SSP2-4.5, moderate mitigation)?

Response:

It has been corrected in the revised manuscript. The text there reads as: "*0.032℃ a^{-1}(SSP2-4.5, moderate mitigation)*".

3. L326: RCP8.5?

Response:

The full text is thoroughly revised and carefully checked to delete errors.

4. Please keep the abbreviation of 'SSPx-y' consistently, e.g., some sentences use SSP1-2.6 (L322), and some sentences use SSP1-26 (L502).

Response:

It has been corrected to the 'SSPx-y.' format throughout the revised manuscript.